JOURNAL OF GEOPHYSICAL RESEARCH, VOL. 113, G03S05, doi:10.1029/2007JG000565, 2008

Modeling biogeophysical interactions in nonsorted circles in the Low Arctic

D. J. Nicolsky,[1] V. E. Romanovsky,[1] G. S. Tipenko,[2] and D. A. Walker[3]

Received 31 July 2007; revised 26 November 2007; accepted 26 February 2008; published 28 May 2008.

[1] We investigate biogeophysical processes that cause differential frost heave in nonsorted circles north of the Alaska's Brooks Range. The main objective is the development of a numerical thermo-mechanical model of a nonsorted circle. The presented model includes mass, momentum and energy conservation laws for water, ice and soil. We applied this model to simulate differential frost heave at the Franklin Bluffs site and obtained a good quantitative agreement with measured dynamics of soil temperature, water content, and frost heave. For other locations such as at the Sagwon Hills and Howe Island sites we obtained qualitative agreement with frost-heave measurements. Sensitivity analysis shows that the most active development of differential frost heave occurs for nonsorted circles within waterlogged areas, as observed in field measurements. For well drained sites, model results and field observations show that the differential frost heave is much smaller in magnitude comparing to that of the water-logged sites. Sensitivity of the model to alternation of the vegetation cover shows that a strong heterogeneity in the vegetation cover promotes active development of the differential frost heave. For nonsorted circles with vegetation on top of the circle, the computed differential heave is less pronounced. The radius of the nonsorted circle influences the magnitude of the frost heave. The computed maximum frost heave in the center of the circle corresponds to 1–1.5 meter diameter nonsorted circles. For nonsorted circles with larger diameters, computed frost heave in the center of a circle is smaller compared to the heave at the circle circumference.

Citation: Nicolsky, D. J., V. E. Romanovsky, G. S. Tipenko, and D. A. Walker (2008), Modeling biogeophysical interactions in nonsorted circles in the Low Arctic, *J. Geophys. Res.*, *113*, G03S05, doi:10.1029/2007JG000565.

1. Introduction

[2] Extensive areas of the Arctic landscape are characteristically patterned into small-scale ground features called nonsorted circles. Nonsorted circles are 0.5 to 3.0 meter diameter patches of barren or sparsely vegetated soil formed by frost action [*van Everdingen*, 2002] and ordinarily develop on poorly drained tundra sites, see Figure 1. These features are associated with development of specific microrelief, vegetation, and soil that strongly affect the active-layer thermal and hydrological properties, and soil microclimate. Therefore, they are an important component of the Arctic landscape. Changes to these systems in relation to changes in climate could affect energy and carbon mass exchange at the tundra surface with possible feedbacks to the climate. However, formation, development, maintenance of such ground patterns and their interaction with vegetation is poorly understood [*Walker et al.*, 2004]. The objective of this study is to numerically model observed frost heave in nonsorted circles and gain understanding of interactions between water fluxes, temperature dynamics as influenced by the plant canopy, and the motion of soil particles and as a result the heave of ground surface.

[3] As a part of the biocomplexity of patterned ground project [*Walker et al.*, 2008], we observed nonsorted circles at several locations near the Dalton Highway in Alaska (Figure 2). We instrumented several nonsorted circles at these sites with sensors that measure soil temperature, moisture content and the maximum frost heave [*Walker et al.*, 2004]. Our measurements revealed that the maximum frost heave in a circle interior was 2 to 8 times greater compared to frost heave of surrounding the circle tundra (see the right plot in Figure 2). This phenomenon is referred to as the differential frost heave. The largest frost heave occurred on poorly drained circles with fine-grained sediments at Franklin Bluffs and Sagwon Hills. In contrast, at a site with near surface gravel deposits and available water supply near West Dock, Alaska North Slope, we observed no signs of nonsorted circle occurrence, and at a well drained site with fine sediment located at Howe Island, we observed "nonheaving" nonsorted circles.

[4] Our field observations support the idea that the frost heave of saturated soil very often cannot be explained solely

[1]Geophysical Institute, University of Alaska Fairbanks, Fairbanks, Alaska, USA.
[2]Institute of Environmental Geoscience, Russian Academy of Science, Moscow, Russia.
[3]Institute of Arctic Biology, University of Alaska Fairbanks, Fairbanks, Alaska, USA.

0148-0227/08/2007JG000565$09.00

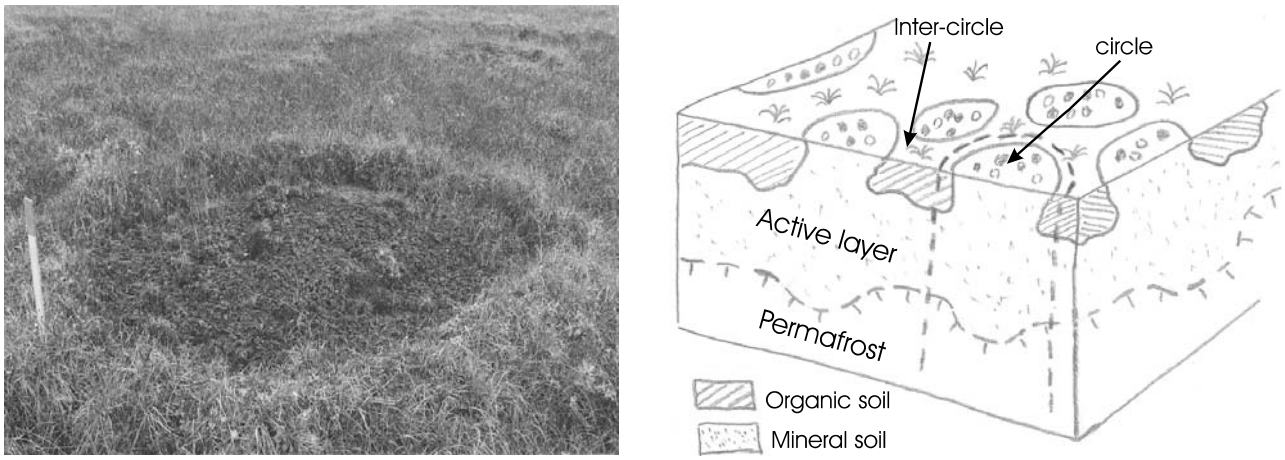

Figure 1. A photography (left) and schematic description (right) of nonsorted circle.

by the expansion of liquid water transforming into ice crystals. It has been shown that under freezing conditions, liquid water can be transported towards the partially frozen soil [*Powers and Helmuth*, 1953; *Litvan*, 1972; *Williams and Smith*, 1989; *Dash et al.*, 1995]. At temperatures below 0°C confined water can partially remain liquid provided that it has lower pressure relative to the adjacent ice, provoking in turn a cryogenic suction of distant water from the unfrozen soil. This type of liquid-water transport has been identified as the driving force of the frost heave [*Taber*, 1918, 1929, 1930]. Other early contributions to frost-heave research are described in *Beskow* [1935]. Although the systematic studies were initiated in 1920s, efforts towards producing predictive tools did not start till decades later. One approach described frost-heave capillary theory based on the Laplace surface tension [*Penner*, 1959; *Everett*, 1961]. Similar ideas were explored in *O'Neill and Miller* [1985] and *Fowler* [1989], where it was suggested that the transport of unfrozen liquid water is due to water pressure gradients arising from temperature-dependent variations in the curvature of the pore ice-water interfaces. In addition to the curvature-pressure model, there are other numerous experimental [*Williams*, 1982; *Watanabe and Mizoguchi*, 2000; *Viklander and Eigenbrod*, 2000] and theoretical [*Konrad and Morgenstern*, 1981; *Wettlaufer and Worster*, 1995; *Li et al.*, 2002; *Peterson and Krantz*, 2003; *Rempel et al.*, 2004; *Coussy*, 2005; *Michalowskin and Zhu*, 2006] studies of freezing ground, but many of them lack description of soil rheology. In this study we apply a general thermo-mechanical model [*Blanchard and Fremond*, 1982; *Fremond and Mikkola*, 1991; *Mikkola and Hartikainen*, 2001] of frost heave to simulate the observed frost heave in nonsorted circles. In this paper, we assume that the soil is a homogeneous mixture of liquid water, ice and soil

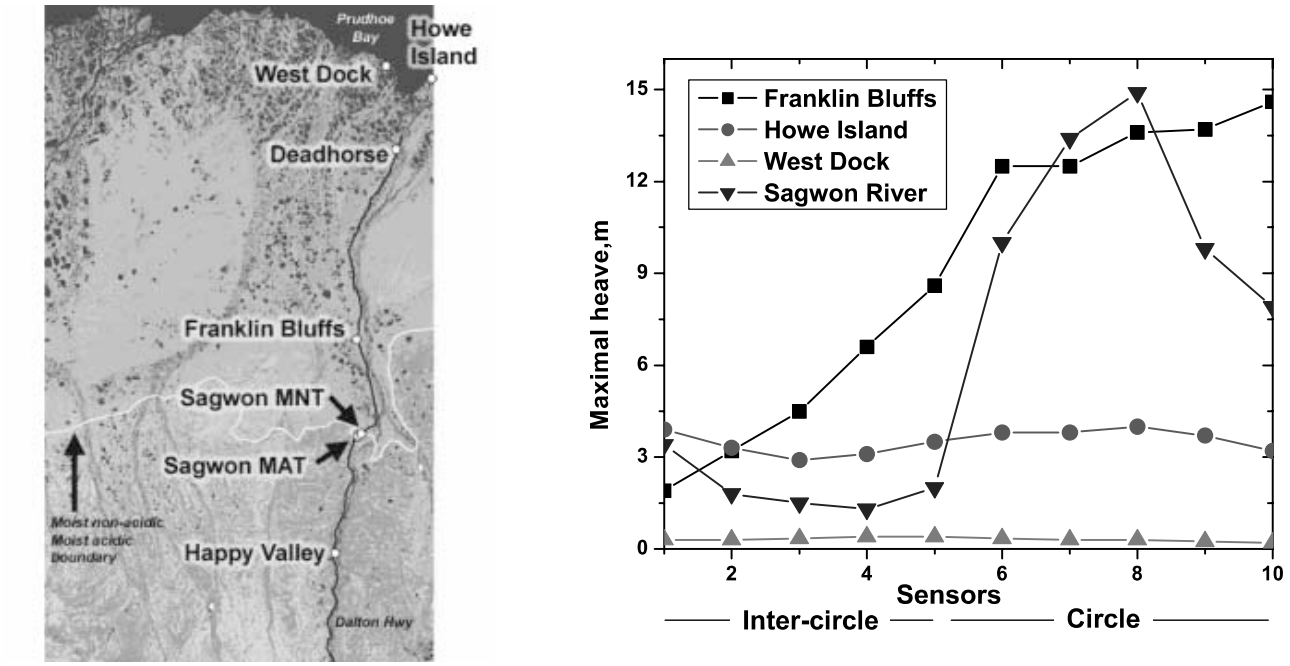

Figure 2. Locations of sites (left) at which several nonsorted circles were monitored. Frost-heave measurements (right) along the cross-section of a nonsorted circle in April 2002.

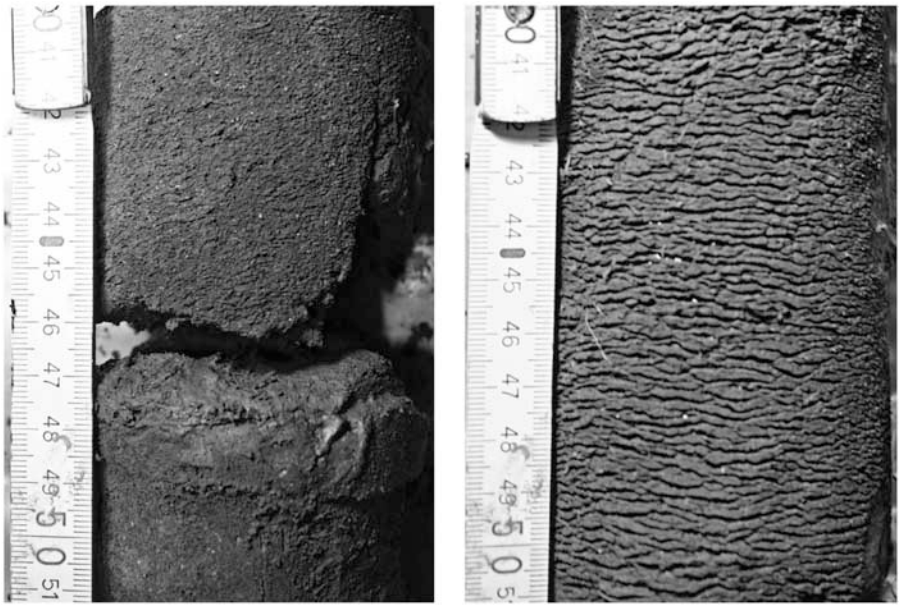

Figure 3. Core samples obtained from the intercircle area (left photo) and circle (right photo) at the Franklin Bluffs site during winter. On the right photograph, a sequence of horizontally oriented ice lenses can be observed. The vertical scale is in centimeters.

skeleton. We assume that the skeleton and ice undergo small deformations described by linear elasticity, and the linear momentum conservation principles can be exploited in the quasi-static from. In our model, we also neglect ice flow relative to the soil skeleton. The body forces due to gravity are neglected too. The liquid water is an incompressible and nonviscous fluid that changes its phase and is always in thermodynamical equilibrium with ice. The chemical potential of the liquid water is modified due to adsorption to the soil skeleton.

[5] Based on observations from field experiments and results of our numerical simulations, we conclude that heterogeneity in surface characteristics and soil properties due to the presence of a heterogeneous plant canopy together with presence of water-logged conditions are among the primarily requirements necessary for occurrence of differential frost heave observed in nonsorted circles. In this article we provide a description of nonsorted circles, a numerical model of the frost heave, and sensitivity study of the developed numerical model. Section-wise this article is organized as follows. In section 2, we highlight key physical processes and mechanisms presumably causing the differential frost heave in nonsorted circles. In section 3, we briefly review a general thermo-mechanical model of soil freezing. In section 4, we summarize the system of governing equations, parametrization of soil properties, and boundary conditions. Section 5 addresses the finite element implementation of the thermo-mechanical model of soil freezing. In section 6, we focus on hydrologically closed systems, in which the cryogenic forces causing the water migration are not considered. In section 7, we analyze effects of the cryogenic suction in hydrologically open and closed systems. In section 8, we apply the model to a specific nonsorted circle located at the Franklin Bluffs site. In section 9, we evaluate sensitivity of the model with respect to soil properties, vegetation cover, and geometrical dimensions of the circles. Finally, in section 10, we provide conclusions and state the main results.

2. Physical Description of Nonsorted Circles and Involved Physical Processes

[6] In this section, we highlight key physical processes and mechanisms presumably causing the differential frost heave in nonsorted circles. Before proceeding to this task we provide some definitions and describe soil thermal, hydrological and rheological properties.

[7] The area surrounding the circle is called the intercircle area and has a relatively thick mat of vegetation as well as a layer of organically enriched soil (see Figure 1). Incorporation of the organic material into soil leads to heterogeneity in thermal properties, structure and water holding capacity of soil. For example, different soil textures indicate distinctive thermal conductivities, soil porosity, and dependence of the unfrozen liquid-water content on temperature. Besides variances in thermal and hydrological properties, the nonsorted circle has heterogeneous rheological properties due to structural change that takes place during annual freeze-thaw cycles. This structural change is caused by freezing water that creates a microscopic structure in a form of a sequence of ice lenses. Figure 3 shows the ice lenses in a soil core samples from a nonsorted circle at the Franklin Bluffs site, Alaska. Each ice lens separates soil particles, causes the observed lenticular soil structure, and hence lessen structural solidity of soil. In *Graham and Au* [1985] and *Qi et al.* [2006], it was shown that soil has a long-term memory of its previous freeze/thaw cycles which in particular reduce bonding between soil particles. To account for reduction in the bonding, we assume that soil is more structurally solid if it has fewer ice lenses. From a soil core obtained by drilling in winter, we observed that the circle has many more ice lenses than in the intercircle area, and these lenses can be found even at the significant

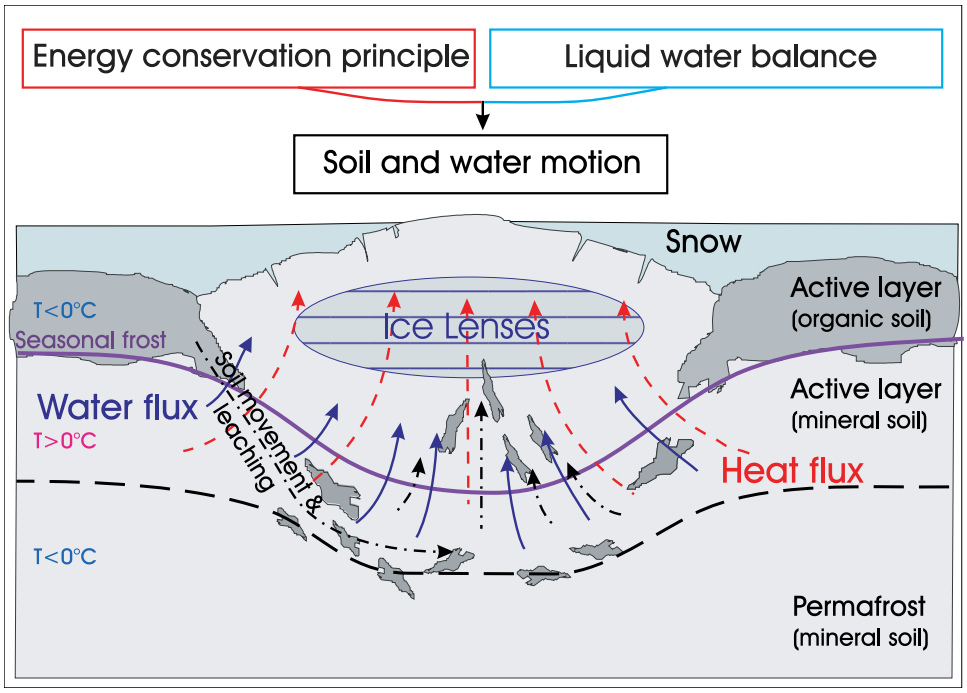

Figure 4. A diagram of fundamental physical processes taking place in a nonsorted circle when it freezes during the fall. Directions of the water flow, heat flux, and soil displacement are marked by blue solid, red dashed and black dot-dashed lines, respectively. Location of the 0 °C isotherm is marked by the solid blue line, whereas location of the permafrost table by the dashed black line.

depth of 0.5 meters (see Figure 3). Therefore, we assume that soil in the intercircle is more structurally solid than in the circle. Despite these heterogeneities, the difference between observed active-layer depths (maximum depth of summer thaw) of the circle and intercircle does not exceed 0.3 meters in the majority of cases.

[8] It is well known that frost heave is caused by volumetric water expansion during freezing. However, as mentioned earlier, the observed frost-heave heights do not seem to be exclusively dependent on the active-layer depth, and on volumetric water content in the soil before freezing. For example, from field observations at the Franklin Bluffs site, we know that the active-layer thicknesses for the circle and intercircle areas are 0.9 and 0.8 meters, respectively, and volumetric water content in these areas during summer is almost the same. Therefore, if water does not migrate, the frost heave is computable and its hight is about 3.0–3.5 cm for both circle and intercircle areas, which contradicts the observations within a circle at Franklin Bluffs site, see Figure 2. Thus, we hypothesize that the key physical process responsible for the differential frost heave is water redistribution in the nonsorted circle due to heterogeneity in soil properties and in ground surface conditions, first of all in vegetation cover. In Figure 4, we show fundamental physical processes occurring in the nonsorted circle in the fall when it freezes. We describe nature of these processes and their implications to the observed values of the differential frost heave as follows.

[9] When the ground surface temperature becomes lower than 0 °C water, trapped in soil pores starts to freeze, in Figure 4 the direction of the heat flux during freezing is shown by red dashed arrows. In several classical works, it was demonstrated that gradual freezing of water at sub-zero temperatures, which takes place under temperature gradients, creates cryogenic suction inducing flow of water towards a freezing region along the temperature gradient [e.g., *O'Neill and Miller*, 1985]. Since the circle lacks an organic layer, frost propagates through it faster, causes stronger water migration into the circle, and consequently results in more intensive ice-lens formation, and results in more frost heave within the circle than in the intercircle area. A secondary consequence of the heave is the reduced thickness of the snowpack above the circle compared to the intercircle area (Figure 4). The heterogeneous snow distribution further enhances the thermal heterogeneity of the soil surface. An absence of a vegetation mat within the heaving areas in conjunction with difference in the snow thickness results in observed lower winter soil temperatures in the circle than in the intercircle. The thermal difference between the circle and intercircle areas affects cryogenic suction and drives water movement from the intercircle to the circle (the direction of liquid-water motion is shown by blue solid arrows). Reaching a freezing region, water forms ice lenses which exert uplifting forces causing deformation of the soil skeleton. We highlight directions of soil particle velocities by black dash-dotted arrows in Figure 4. In our model we exploit a simplest rheological model of the soil skeleton and assume that its deformations are well simulated by linear elasticity theory, in which the soil stiffness takes into account structural differences and lessened soil bonding caused by the ice lenses.

[10] Besides the thermal differences which cause liquid-water migration towards the circle, hydraulic properties of the soil also determine a water flux affecting the liquid-water migration. One of the key hydraulic parameters is a coefficient of hydraulic conductivity k_h and its dependence

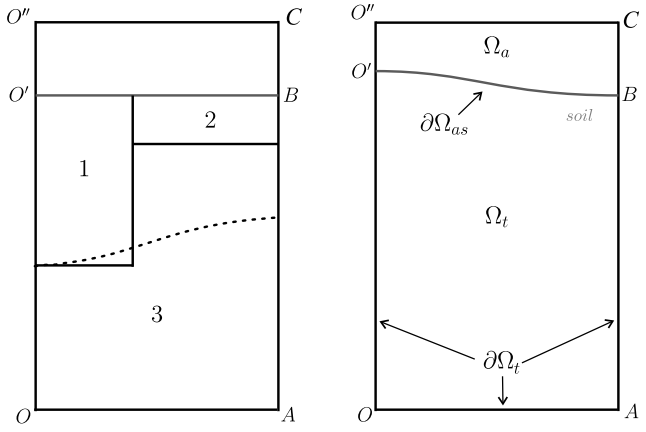

Figure 5. The schematic cross section (left) of the nonsorted circle and its computational domain (right). Segment OO'' is the axis of rotation, AB is the external boundary, and the dotted line on the left shows the upper permafrost boundary. Domains 1 and 3 - mineral soil, Domain 2 - organic soil. Regions Ω_a and Ω_t represent air and soil, respectively. The segment $\partial\Omega_{as}$ is the ground surface. The boundary $\partial\Omega_t$ is the boundary of the computational domain associated with the nonsorted circle.

on unfrozen water content for partially frozen ground. In this study we exploit parametrization of k_h given by

$$k_h = k_0 \theta_w^{\alpha}, \tag{1}$$

where k_0 is the hydraulic conductivity of the thawed soil, θ_w is the volumetric liquid-water content and $\alpha \in [3, 9]$ [*Konrad and Duquennoi*, 1993]. Analyzing this formula we conclude that the hydraulic conductivity k_h increases with an increase of unfrozen water content θ_w, a function of both temperature and porosity. Another hydrological soil property that is important to sustain water migration is the availability of water inside the nonsorted circle or at its boundary. Note that from observations it is known that the higher values of frost heave have been measured at poorly drained sites. Therefore, lateral boundary conditions play an important role in allowing water to migrate into the circle due to cryogenic suction and to create ice lenses. In our model, we simulate the nonsorted circles either as hydrologically open or closed systems by setting to zero either the pressure or water flux on external boundaries, respectively. In the next section, we will briefly describe the general thermo-mechanical model of freezing soil. An interested reader can consult other works, where the theory is discussed in detail [*Hartikainen and Mikkola*, 1997; *Mikkola and Hartikainen*, 2001; *Jussila*, 2006].

3. Review of a General Thermo-Mechanical Model of Soil Freezing

[11] We consider a mixture of several constituents: water w, ice i and soil s particles occupying a region Ω_t in space at time t, see right plot in Figure 5. We assume that at each point of Ω_t constituents coexist with each other and each of them occupies a part V_k, $k \in \{w, i, s\}$ of a representative volume V in Ω_t. We mark all quantities related to the k-th constituent with subscript k and denote by θ_k the volume fraction satisfying $\theta_k V = V_k$. Note that the nonnegative volume fractions also satisfy the so-called saturation condition

$$\theta_i + \theta_w + \theta_s = 1, \tag{2}$$

or equivalently $\eta + \theta_s = 1$, where $\eta = \theta_w + \theta_i$ is called the soil porosity. Assuming that all constituents are incompressible, the density ρ_k is equal to $\bar{\rho}_k \theta_k$, where $\bar{\rho}_w = 1000$, $\bar{\rho}_i = 900$, and $\bar{\rho}_s$ is a constant depending on the soil type. (We assume units for all types of physical quantities in S.I. system of units, unless it is otherwise stated.)

[12] Denoting by $\boldsymbol{v}_k$ the spatial velocity, we formulate mass conservation principles for water, ice and soil particles as follows

$$\begin{aligned} &\frac{\partial \rho_w}{\partial t} + \nabla\cdot(\rho_w \boldsymbol{v}_w) = \hat{\rho}, \\ &\frac{\partial \rho_i}{\partial t} + \nabla\cdot(\rho_i \boldsymbol{v}_i) = -\hat{\rho}, \\ &\frac{\partial \rho_s}{\partial t} + \nabla\cdot(\rho_s \boldsymbol{v}_s) = 0, \end{aligned} \tag{3}$$

where $\hat{\rho}$ is the rate of mass exchange between liquid water and ice. Note that the quantity $\hat{\rho}$ is not zero only during freezing or thawing, when phase change between water and ice occurs. Taking into account that soil particles and ice move with the same velocity $\boldsymbol{v}_i = \boldsymbol{v}_s = \boldsymbol{v}$, we combine equations in (3) to derive

$$\nabla \cdot (\theta_w(\boldsymbol{v}_w - \boldsymbol{v})) + \nabla \cdot \boldsymbol{v} = -\gamma \frac{\hat{\rho}}{\bar{\rho}_i}, \qquad \gamma = 1 - \frac{\bar{\rho}_i}{\bar{\rho}_w}. \tag{4}$$

One of the variables in the water mass conservation laws (4) is $\boldsymbol{v}$, which can be calculated taking into account soil rheology. Since the ground heaves slowly with $||\boldsymbol{v}|| \ll 1$, the velocity $\boldsymbol{v}$ can be approximated by $\boldsymbol{v} = \frac{\partial}{\partial t}\boldsymbol{u}$, where $\boldsymbol{u}$ is the displacement of soil particles, satisfying a quasi-static linear momentum conservation principle

$$\nabla \cdot \boldsymbol{\sigma} = 0, \qquad \boldsymbol{\sigma} = \hat{\boldsymbol{\sigma}} - \boldsymbol{I}P \tag{5}$$

where $\boldsymbol{\sigma}$ is the total stress tensor, $\hat{\boldsymbol{\sigma}}$ is the effective stress tensor, P is the pore pressure, and $\boldsymbol{I}$ stands for the identity second order tensors. Assuming that the soil is isotropic and undergoes small deformations, we approximate the effective stress tensor $\hat{\boldsymbol{\sigma}}$ as follows

$$\begin{aligned} &\hat{\boldsymbol{\sigma}} = \frac{E}{1+\nu}\left(\boldsymbol{\epsilon} + \frac{\nu}{1-2\nu}\mathrm{tr}(\boldsymbol{\epsilon})\boldsymbol{I}\right), \\ &\mathrm{tr}(\boldsymbol{\epsilon}) = \nabla \cdot \boldsymbol{u}, \\ &\boldsymbol{\epsilon} = \frac{1}{2}\left(\nabla \boldsymbol{u} + (\nabla \boldsymbol{u})^t\right), \end{aligned} \tag{6}$$

where $\boldsymbol{\epsilon}$ is the strain tensor, E and ν are the Young's modulus and Poisson's ratio of the soil, respectively. Here, the symbol t denotes the transpose operator.

[13] Pore pressure P is defined in *Mikkola and Hartikainen* [2001] as

$$P = \sum_{k \in \{i,w,s\}} p_k, \tag{7}$$

where p_k is the thermodynamics pressure defined accordingly to

$$p_k = \theta_k \sum_{j\in\{w,i,s\}} \rho_j \frac{\partial \psi_j}{\partial \theta_k},$$

where ψ_k is the Hemlhotz free energy [*Landau and Lifshitz*, 1969]. Considering a certain ansatz for the Hemlhotz free energy it is possible to derive that

$$p_k = \theta_k \left[\rho_w \frac{LT}{T_0} \frac{\partial f}{\partial \theta_k} + p \right], \tag{8}$$

where p can be considered as hydrostatic type of pressure, T is the soil temperature, T_0 is the temperature of water fusion and is 273.15 K, L is the latent heat of fusion, and f is a certain function of volume fractions described later in the article. A detailed discussion regarding the physical meanings of commonly occurring pressure terms p_k, p can be found in *Bennethum and Weinstein* [2004]. Let us note that from a physical point of view the hydrostatic pressure p means restriction (2) of interpenetration of the constituents through each other [*Fremond and Mikkola*, 1991]. Also, we emphasize that from (8) it is possible to derive a well-known relationship

$$\frac{p_w}{\theta_w} - \frac{p_s}{\theta_s} = \rho_w \frac{LT}{T_0} \left[\frac{\partial f}{\partial \theta_w} - \frac{\partial f}{\partial \theta_s} \right]$$

for a binary model consisting liquid and solid. The right hand side can be interpreted as the surface tension of water in the pores.

[14] The expression for the function f is based on the following arguments. Inside a pore, water is bound to the soil particles with the strength decreasing with distance from the pore wall. In terms of energy, it is possible to state that the energy of water decreases with distance from the soil particle [*Hobbs*, 1974; *Tsytovich*, 1975], or equivalently the more strongly bound water requires a lower temperature to freeze it. Therefore, freezing begins in the middle of the pore where the water is less bound and advances towards the pore walls while the temperature decreases. From private communications with J. Hartikainen and from *Mikkola and Hartikainen* [2001], the general shape of the function f should fulfill the following requirements: f increases as θ_w decreases and goes to infinity as θ_w approaches zero. This implies that the a certain layer of the adsorbed water remains unfrozen for all temperatures. In the work of *Mikkola and Hartikainen* [2001], the function f is given by

$$f(\chi) = a\left(\frac{1}{\chi} - 1\right)^2, \qquad \theta_w = \chi\eta \tag{9}$$

where the constant a can be determined by the Clapeyron relations. In the case of $|T - T_0| \ll T_0$, the Clapeyron relation is given by

$$[L + (C_w - C_i)(T - T_0)] \frac{T - T_0}{T_0} + \gamma \frac{p}{\bar{\rho}_i} = L \frac{T}{T_0} \left(f + \chi \frac{\partial f}{\partial \chi} \right), \tag{10}$$

where C_w and C_i are the specific heat capacity of water and ice, respectively. This equation gives the relationship between the temperature T, the pressure p, the porosity n, and the relative water content χ. Assuming that pressure variations in the freezing soil are relatively small to influence the unfrozen liquid water content, we suppose that χ does not depend on the pressure p in (10). Substituting (9) into (10), we derive that

$$\chi = \left[1 - \frac{1}{a} \left(1 + \frac{(C_w - C_i)(T - T_0)}{L} \right) \frac{T - T_0}{T} \right]^{-\frac{1}{2}} \tag{11}$$

for $T < T_0$, and is equal to 1 for $T \geq T_0$. This formula can also be used for experimental verification of the function f [*Hartikainen and Mikkola*, 1997].

[15] Returning to the mass conservation principle for water (4), we express the velocity of water relative to soil particles by the generalized Darcy's law:

$$\theta_w(\boldsymbol{v}_w - \boldsymbol{v}) = -\frac{k_h}{g\bar{\rho}_w} \left(\nabla\left(\frac{p_w}{\theta_w}\right) + \bar{\rho}_w \frac{LT}{T_0} \nabla f \right),$$

or

$$\theta_w(\boldsymbol{v}_w - \boldsymbol{v}) = -\frac{k_h}{g\bar{\rho}_w} (\nabla p + \mathcal{F}),$$
$$\mathcal{F} = \bar{\rho}_w L \left(\nabla\left(\theta_w \frac{T}{T_0} \frac{\partial f}{\partial \theta_w}\right) + \frac{T}{T_0} \nabla f \right), \tag{12}$$

where g is the gravitational acceleration, and the quantity $\mathcal{F}$ is a water flux due to the matric potential described in *Huyghe et al.* [2004]. Note, in Terzaghi's consolidation theory the matric potential $\mathcal{F}$ is not considered. The quantity $\mathcal{F}$ vanishes in a homogeneous medium where variations in θ_w are small and the pore structure is coarse. However, near the 0°C isoline where freezing occurs, there is a large gradient of liquid-water content θ_w, and consequently the value of $\mathcal{F}$ has to be taken into account.

[16] Since the flux $\mathcal{F}$ depends on temperature, we consider the energy conservation principle for the entire mixture

$$L\hat{\rho} + C \frac{\partial T}{\partial t} = \nabla \cdot (\lambda \nabla T). \tag{13}$$

Here, C is the volumetric heat capacity, λ is the thermal conductivity, and the quantity $\hat{\rho}$ is calculated by exploiting the second and third equations in (3):

$$\hat{\rho} = \bar{\rho}_i \left(\frac{\partial \theta_w}{\partial t} - \nabla \cdot ((1 - \theta_w)\boldsymbol{v}) \right). \tag{14}$$

Note that for unfrozen soil θ_w is equal to η, whereas for partially frozen ground $\theta_w < \eta$ and is given by the unfrozen water content curve. This curve specifies the temperature dependence of θ_w in partially frozen ground.

4. System of Governing Equations, Parametrization of Soil Properties, and Boundary Conditions

[17] In this section we derive a system of governing equations, which is solved by the finite element method [*Zienkiewicz and Taylor*, 1991] in a certain domain. Since a nonsorted circle has an axial symmetry, we solve the

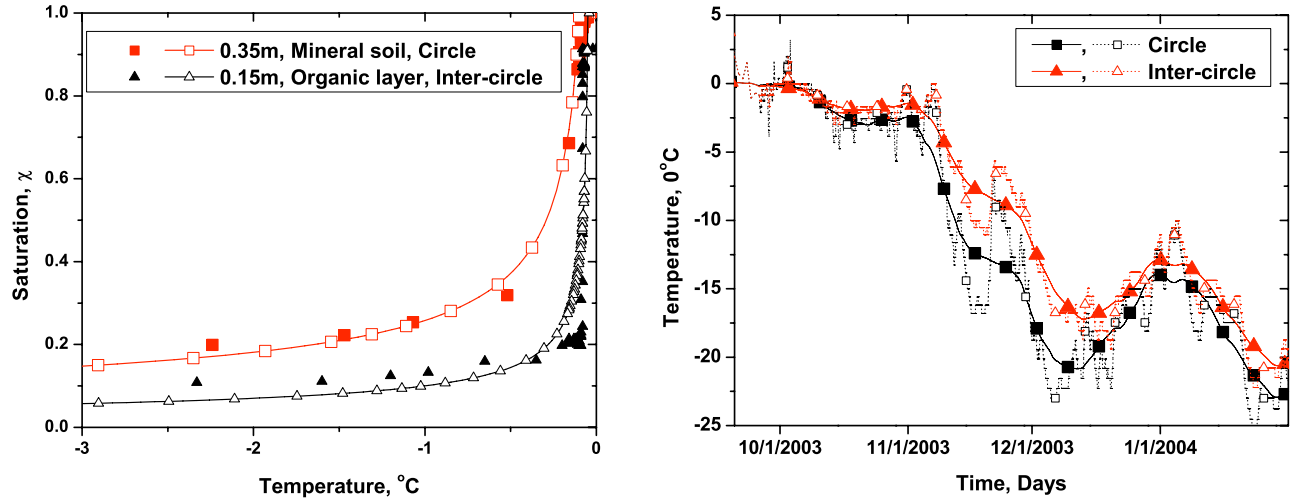

Figure 6. In the left plot, calibration of the unfrozen water content curve by fitting (hollow symbols) $\chi(T)$ expressed from (11) to the measured data (filled symbols). In the right plot, temperature dynamics $T_{surface}^{circle}$, $T_{surface}^{intercircle}$ on the surface of the nonsorted circle at the center of the circle and in the intercircle, respectively. The time series $T_{surface}^{circle}$ and $T_{surface}^{intercircle}$ are records (the five day averaged, filled symbols, solid line) of ground surface temperatures measured (dotted line, hollow symbols) at 0.01 meter depth.

governing equations in a 2-D domain, shown in the left plot in Figure 5. It is the radial cross-section of nonsorted circle from circle's axis of rotation OO' to a lateral boundary AB located in the intercircle. The circle does not have organically enriched soil and consists of only mineral soil that is marked by 1. To describe soil structure in the intercircle, we mark an organically enriched layer by number 2, and the mineral soil below it by 3.

[18] We exploit the heat equation (13), mass exchange relationship (14) and $\theta_w = \theta_w(T, \eta)$ to obtain an equivalent form of the heat equation:

$$C\frac{\partial T}{\partial t} + \bar{\rho}_i L\left(\frac{\partial \theta_w}{\partial T}\frac{\partial T}{\partial t} + \left(\frac{\partial \theta_w}{\partial \eta} - 1\right)\frac{\partial \eta}{\partial t}\right) = \nabla\cdot(\lambda\nabla T) + \rho_i L\nabla\cdot\left(\alpha\frac{\partial \boldsymbol{u}}{\partial t}\right), \tag{15}$$

where $\alpha = \eta - \theta_w$ is non zero only for partially frozen soil. Introducing $\beta = \alpha\gamma - 1$, we substitute terms in the mass conservation principle (4) by expressions given in (12) and (14) to obtain an equation with respect to pore pressure p:

$$\gamma\left(\frac{\partial \theta_w}{\partial T}\frac{\partial T}{\partial t} + \left(\frac{\partial \theta_w}{\partial \eta} - 1\right)\frac{\partial \eta}{\partial t}\right) = \nabla\cdot\left(\frac{k_h}{g\bar{\rho}_w}(\nabla p + \mathcal{F})\right) + \nabla\cdot\left(\beta\frac{\partial \boldsymbol{u}}{\partial t}\right). \tag{16}$$

The above equation is supplemented by an equation

$$\nabla\cdot\hat{\boldsymbol{\sigma}} = \nabla P, \tag{17}$$

which relates the hydrostatic pressure p and deformation $\boldsymbol{u}$. Note that the equation pair ((16)–(17)) is commonly occurring in quasi-static poroelasticity theory. Finally, we include the mass conservation principle for the soil skeleton

$$\frac{\partial \eta}{\partial t} - \nabla\cdot\left((1-\eta)\frac{\partial \boldsymbol{u}}{\partial t}\right) = 0 \tag{18}$$

with respect to soil porosity $\eta = 1 - \theta_s$ in order to close the above system of equations.

[19] Depending on the choice of parameters λ, k_h, a, E, and C in ((16)–(18)), it is possible to simulate freezing of various types of soil. However, since we are interested in modeling of nonsorted circles, we provide typical values of these parameters listed in Table 1 for sites along the Dalton Highway in Alaska. Besides the typical values, it is also important how these parameters are parameterized. In equation (15), the thermal conductivity λ and the volumetric heat capacity C are expressed according to *de Vries* [1963]:

$$C = \rho_s C_s + \rho_w C_w + \rho_i C_i, \qquad \lambda = \lambda_s^{\theta_s}\lambda_w^{\theta_w}\lambda_i^{\theta_i},$$

where C_k and λ_k are the specific heat capacities and thermal conductivities, respectively. With respect to the rheological properties E and ν, we assume that the soil is consolidated, and hence the Young's modulus E for soil compression is twice as large as for its tension. Also, since area 3 has fewer ice lenses than areas 1 and 2, area 3 is more structurally solid and has a larger value of Young's modulus E. To find the value of the constant a in (9), we exploit the formula (11) to express θ_w as a function of temperature and fit it to the measured unfrozen water content, see the left plot in Figure 6.

[20] In order to solve the above system ((16)–(18)) of partial differential equations, it usually has to be supplemented by certain boundary conditions specified at the ground surface, some depth, and at lateral boundaries of the nonsorted circle. Before describing the boundary con-

Table 1. Description and Range of Soil Properties Values for Nonsorted Circles Along the Dalton Highway in Alaska

Domain	Soil	Ice Lenses	Unfrozen Water	λ_s	$E \cdot 10^6$	a
1	Mineral	Many	High content	0.9...1.9	1...5	$1 \cdot 10^{-4}$
2	Organic	Many	Low content	0.3...0.8	1...5	$1 \cdot 10^{-5}$
3	Mineral	Few	High content	0.9...1.9	10...50	$1 \cdot 10^{-4}$

ditions, we recall that a single nonsorted circle is an axisymmetrical cylindrical object. Therefore, in order to reduce computational time, we model frost-heave dynamics in a 2-D domain with the axial symmetry. In Figure 5, right plot, we show a 2-D computational domain Ω_t associated with nonsorted circle and with an axis of rotation marked by OO'. We formulate the boundary conditions with respect to pressure, temperature, and soil particle displacement on the axis OO', the ground surface $\partial\Omega_{as}$, at the lateral boundary AB and at some depth OA as follows.

[21] First, we consider boundary conditions with respect to temperature T. We assume that the lateral boundary AB is located far away from the circle, and there is no lateral heat flow, i.e. $\boldsymbol{\nu}\cdot(\lambda\nabla T) = 0$, where $\boldsymbol{\nu}$ is the outward normal vector to the boundary. At the axis of rotation OO' due to symmetry principle, we impose no heat flux boundary conditions. At the ground surface $\partial\Omega_{as}$ and some depth OA the temperature is set according to its measured values. Our field observations reveal that the ground surface temperatures within a circle area is constant in lateral directions and is significantly different from the temperature in the intercircle. Also, we note that during the freezing period there is a jump in ground surface temperature at the border between the circle and the intercircle (see Figure 6). Thus, we specify the ground surface temperature at intercircle and circle by $T^{circle}_{surface}(t)$, and $T^{intercircle}_{surface}(t)$, respectively. These temperatures were measured at 0.01 meter depth below the surface of mineral soil in the circle, and 0.01 meters below the surface of organic mat in the intercircle. In Figure 6, we plot temperature dynamics of $T^{circle}_{surface}(x,t)$ and $T^{intercircle}_{surface}(t)$. Note that the temperature $T^{circle}_{surface}(t)$ is typically colder than $T^{intercircle}_{surface}(t)$, since the circle has a thinner snow and no vegetation cover comparing to the intercircle.

[22] Second, we specify boundary conditions with respect to pressure p. Below, in section 7, we show that this boundary conditions plays a decisive role in determining frost-heave dynamics. Two standard boundary conditions for the pressure p are the Neumann, $\boldsymbol{\nu}\cdot\nabla p = 0$, and the Dirichlet, $p = 0$, boundary conditions. It is possible to check that if $\boldsymbol{\nu}\cdot\nabla p = 0$ and $\boldsymbol{\nu}\cdot\nabla T = 0$ are simultaneously specified on the boundary, then this boundary is water impermeable, and the condition $\boldsymbol{\nu}\cdot\theta_w(\boldsymbol{v} - \boldsymbol{v}_w) = 0$ holds. On the other hand $p = 0$ models water permeable boundary but also leads to an additional force term into total stresses $\boldsymbol{\sigma}$ on the boundary and consequent soil deformations. The pore pressure boundary condition $P = 0$ would be more realistic than $p = 0$, but its implementation would require to overcome certain difficulties. Since we are interested in modeling the differential frost heave between the circle and intercircle, we impose the lateral boundary condition on AB that is "far away" from the circle, i.e. all disturbances caused by $p = 0$ on the lateral boundary would not affect the solution in the circle.

[23] For example, if liquid water is abundant in the area surrounding the nonsorted circle and it can flow into the nonsorted circle, then we model water-permeable boundary conditions by setting $p = 0$ on the lateral boundary AB. However, if additional water is scarce or not available, and a flow of water into the nonsorted circle is negligibly small, then the water-impermeable boundary condition $\boldsymbol{\nu} \cdot \theta_w(\boldsymbol{v} - \boldsymbol{v}_w) = 0$ on AB is modeled by setting $\boldsymbol{\nu} \cdot \nabla p = 0$ on AB. We note that $\boldsymbol{\nu}\cdot\nabla T = 0$ is always set on AB because there is no heat flux across the lateral boundary. Thus, we define a system to be open if $p = 0$ is set on AB, and closed if $\boldsymbol{\nu} \cdot \theta_w(\boldsymbol{v} - \boldsymbol{v}_w) = 0$ is modeled on AB. On the axis OO' and OA we set no water flux boundary conditions. At the surface $\partial\Omega_{as}$, we assume that water can flow in and out of the domain Ω_t, i.e. $p = 0$ on $\partial\Omega_{as}$.

[24] Third, we describe boundary conditions with respect to displacement of soil particles. Since there are no physical loads applied to the ground surface and it can move freely, we set $\boldsymbol{\sigma}\cdot\boldsymbol{\nu} = 0$ on $\partial\Omega_{as}$. On the lateral boundary AB, far away from the circle, we assume that the soil particles can move freely in vertical direction, but not in the horizontal one. Therefore, $u_r = 0$, $(\boldsymbol{\sigma}\cdot\boldsymbol{\nu})_z = 0$ is set on AB. Due to symmetry we impose the same boundary condition on the axis of rotation OO': i.e. $u_r = 0$, $(\boldsymbol{\sigma}\cdot\boldsymbol{\nu})_z = 0$. Note that since the segment OA is located in permafrost, no soil motion can occur, and hence $\boldsymbol{u} = 0$. We summarize all boundary conditions in Table 2.

5. Finite Element Formulation and the Fictitious Domain Method

[25] At any time t, the mixture of water and soil particles occupying a domain Ω_t undergoes deformation, which leads to dynamic geometry of Ω_t. One of the techniques to solve the system of equations ((16)–(18)) in the changing-in-time domain Ω_t is to implement the fictitious domain method [*Glowinski et al.*, 1994]. Following this ideology, we embed Ω_t into a larger fixed-in-time rectangle domain Ω [*Buzbee et al.*, 1971], area $OO''CA$ in Figure 5, right plot. A supple-

Table 2. Boundary Conditions

Variable	AB	$\partial\Omega_{as}$	OA	OO'
T	$\boldsymbol{\nu} \cdot (\lambda\nabla T) = 0$	$T = T_{surface}$	$T = T_{bottom}$	$\boldsymbol{\nu} \cdot (\lambda\nabla T) = 0$
P	$\boldsymbol{\nu} \cdot \theta_w(\boldsymbol{\nu} - \boldsymbol{\nu}_w) = 0$, or $P = 0$	$P = 0$	$\boldsymbol{\nu} \cdot \theta_w(\boldsymbol{v} - \boldsymbol{\nu}_w) = 0$	$\boldsymbol{\nu} \cdot \theta_w(\boldsymbol{v} - \boldsymbol{v}_w) = 0$
$\boldsymbol{u}$	$u_r = 0$, $(\boldsymbol{\sigma} \cdot \boldsymbol{\nu})_z = 0$	$\boldsymbol{\sigma} \cdot \boldsymbol{\nu} = 0$	$\boldsymbol{u} = 0$	$u_r = 0$, $(\boldsymbol{\sigma} \cdot \boldsymbol{\nu})_z = 0$

ment of Ω_t in Ω is called the fictitious domain $\Omega_a = \Omega \backslash \Omega_t$. From the physical point of view Ω_a is related to air which is being displaced by heaving ground. Note that as the soil surface heaves, some fixed points in Ω_a initially representing air are to be associated with soil Ω_t. Therefore, the initial height of Ω_a has to be taller than the maximum displacement of the ground surface $\partial\Omega_{as}$ relative to its position prior to any heaving. An advantage of implementing the fictitious domain method is that the time consuming triangulation of Ω_a into triangles $\{\mathcal{K}\}$ is completed only once. A second advantage is that we solve the same set of equations ((15)–(18)) in both domains Ω_t and Ω_a.

[26] We implement a standard finite element method [*Zienkiewicz and Taylor*, 1991] and partition the domain Ω into regular nonoverlapping triangles $\{\mathcal{K}\}$ with vertices at $\{x_i\}_{i=1}^m$. We consider piece-wise linear continuous functions $\{\varphi_i(x) : x \in \Omega\}_{i=1}^m$, such that $\varphi_i(x_j) = \delta_{ij}$, $i, j = 1, \ldots, m$, and $\varphi_i(x)$ is linear on each triangular. We expand physical variables T, p, θ_s and $\boldsymbol{u}$ in a basis of $\{\varphi_i\}$:

$$\mathcal{P}(x,t) \approx \sum_{i=1}^{m} \varphi_i(x)\mathcal{P}_i(t), \qquad x \in \boldsymbol{\Omega}, \qquad t \geq 0, \tag{19}$$

where $\mathcal{P}$ is one of the physical variables, and $\mathcal{P}_i$ is the value of $\mathcal{P}$ at the ith node associated with x_i. Therefore the system of equation ((15)–(18)) can be discretized to form the following nonlinear system of differential equations

$$\mathbf{M}(\mathbf{X}(t))\frac{\partial \mathbf{X}(t)}{\partial t} = \mathbf{K}(\mathbf{X}(t))\mathbf{X}(t) + \mathbf{F}(t), \qquad \mathbf{X}(0) = \mathbf{X}_0 \tag{20}$$

where $\mathbf{M}$ and $\mathbf{K}$ are sparse nonsingular matrices, and $\mathbf{X}$ is a vector containing values of all physical variables at all nodes. To solve the system in (20) we utilize an implicit time scheme and Picard iterations [*Samarskii and Vabishchevich*, 1996]

$$\begin{aligned} &\mathbf{M}(\mathbf{X}_{n+1})(\mathbf{X}_{n+1} - \mathbf{X}_n) = \Delta t_n(\mathbf{K}(\mathbf{X}_{n+1})\mathbf{X}_{n+1} + \mathbf{F}(\mathbf{X}_{n+1})), \\ &\mathbf{X}_n = \mathbf{X}(t_n), \end{aligned} \tag{21}$$

where t_n is the time at the n^{th} time step, and $\Delta t_n = t_{n+1} - t_n$ is the time increment. Given $\mathbf{X}_n$, we solve the nonlinear equation (21) with respect to $\mathbf{X}_{n+1}$ by iterations $s = 0,1, \ldots, s_0$. The iterations are started by the initial guess $\mathbf{X}_{n+1}^0 = \mathbf{X}_n$ and are terminated at s_0 when certain convergence criteria are met. The previous approximation $\mathbf{X}_{n+1}^s$ is used to compute the consecutive one $\mathbf{X}_{n+1}^{s+1}$ as follows. The value of $\mathbf{X}_{n+1}^s$ is used to evaluate the matrices $\mathbf{K}(\mathbf{X}_{n+1}^s)$ and $\mathbf{M}(\mathbf{X}_{n+1}^s)$ and the vector $\mathbf{F}(\mathbf{X}_{n+1}^s)$, which are then utilized to compute the solution $\mathbf{X}_{n+1}^{s+1}$ of

$$\mathbf{M}\big(\mathbf{X}_{n+1}^s\big)\big(\mathbf{X}_{n+1}^{s+1} - \mathbf{X}_n\big) = \Delta t_n\big(\mathbf{K}\big(\mathbf{X}_{n+1}^s\big)\mathbf{X}_{n+1}^{s+1} + \mathbf{F}\big(\mathbf{X}_{n+1}^s\big)\big)$$

at $s + 1$ iteration. At each iteration the convergence criteria $\max_i|T_{n+1,i}^{s+1} - T_{n+1,i}^s| \leq \epsilon_1$ and $\max_i||\boldsymbol{u}_{n+1,i}^{s+1} - \boldsymbol{u}_{n+1,i}^s|| \leq \epsilon_2$, is checked, where $\epsilon_1, \epsilon_2 > 0$. If it holds, iteration is terminated at $s_0 = s_{n+1}$. If the number of iterations exceeds a certain number then the time increment Δt_n is halved. The convergence criteria is always reached if the time increment Δt_n is small enough [*Samarskii and Vabishchevich*, 1996].

[27] Since the domain Ω_t is embedded into a larger domain Ω, we are not able to set boundary conditions on $\partial\Omega_{as}$ directly, since it is immersed in Ω. In the framework of the fictitious domain method, one of the ways to resolve this problem is given as follows [*Buzbee et al.*, 1971; *Astrakhantcev*, 1978; *Marchuk et al.*, 1986]. First, we set certain boundary conditions on $\partial\Omega_a$ and then specify coefficients in ((15)–(17)) such that we have the conditions, listed in Table 2 on the surface $\partial\Omega_{as}$.

[28] We deal with setting $T = T_{surface}$ on $\partial\Omega_{as}$ as follows. Note that the thermal conductivity λ is a positive scalar. Generally, however, it can be any positive definite matrix. Therefore, in order to set $T = T_{surface}$ on $\partial\Omega_{as}$, we impose $T = T_{surface}$ on the boundary $O''C$ (Figure 5, right) and set $L = 0$, $\lambda = \mathrm{diag}(\lambda_x, \lambda_y)$ in Ω_a, where $0 < \lambda_x \ll$ and $1 \ll \lambda_y$ [*Saulev*, 1963; *Kuznetsov*, 2000; *Sergueev et al.*, 2003]. Equivalent to setting the temperature on the ground surface $\partial\Omega_{as}$, we restrict the pressure $p = 0$ on $\partial\Omega_{as}$ by letting $\rho_i = \rho_w$, $L = 0$ and $k_h \gg 1$ in Ω_a, and putting $p = 0$ on segments OO'', $O''C$ and CB. Modeling $\boldsymbol{\sigma}\cdot\boldsymbol{\nu} = 0$ on $\partial\Omega_{as}$ is done similarly to an approach described in *Ramiere et al.* [2005] by imposing the traction free boundary conditions $\boldsymbol{\sigma}\cdot\boldsymbol{\nu} = 0$ on $\partial\Omega_f$, a small Young's modulus $0 < \mathrm{E} \ll 1$ and zeroing out the internal body forces in the fictitious domain Ω_a.

[29] Finally, we consider the continuity equation (18). Since there are no internal body forces in Ω_a and $\boldsymbol{\sigma}\cdot\boldsymbol{\nu} = 0$ is on $\partial\Omega_a$ and $\partial\Omega_s$, $\boldsymbol{\sigma} = 0$ holds in Ω_a. Therefore, $\nabla\cdot\boldsymbol{u} = 0$ is in Ω_a. Taking a time derivative, we obtain $\nabla\cdot\boldsymbol{v} = 0$, and hence the mass continuity equation (18) becomes an advection equation in Ω_a:

$$\frac{\partial \theta_s}{\partial t} + v\nabla\theta_s = 0.$$

Note that during freezing, the ground heaves and $\boldsymbol{v}\cdot\boldsymbol{\nu} \geq 0$, where $\boldsymbol{\nu}$ is an outward normal vector to Ω_t on the surface $\partial\Omega_{as}$. Therefore, the characteristics defined by $\boldsymbol{v}$ point outside the domain Ω_t, and hence θ_s in Ω_s does not depend on θ_s in Ω_a.

6. Hydraulically Closed System, No Suction

[30] In this and the following sections, we analyze the model both quantitatively and qualitatively. Since dependence of the frost-heave dynamics on thermal, hydraulic and rheological properties and boundary conditions is rather complicated, we consider several particular cases. In this section, we model frost heave of soils in which migration of water towards the freezing region is not considered, or $\mathcal{F} = 0$. With this condition, the system ((16)–(17)) becomes

$$\gamma\frac{\partial \theta_w}{\partial t} = \nabla\cdot\left(\frac{k_f}{g\bar{\rho}_w}\nabla p\right) + \nabla\cdot\left(\left(\frac{\bar{\rho}_i}{\bar{\rho}_w} + \gamma\theta_w\right)\frac{\partial \boldsymbol{u}}{\partial t}\right), \quad \nabla\cdot\hat{\boldsymbol{\sigma}} = \nabla p. \tag{22}$$

From the physical point of view, the left hand side of the first equation describes the rate of water volume change during freezing or thawing. For example, during freezing water expands and "some material is being injected" into the soil skeleton, which results in the pressure increase and

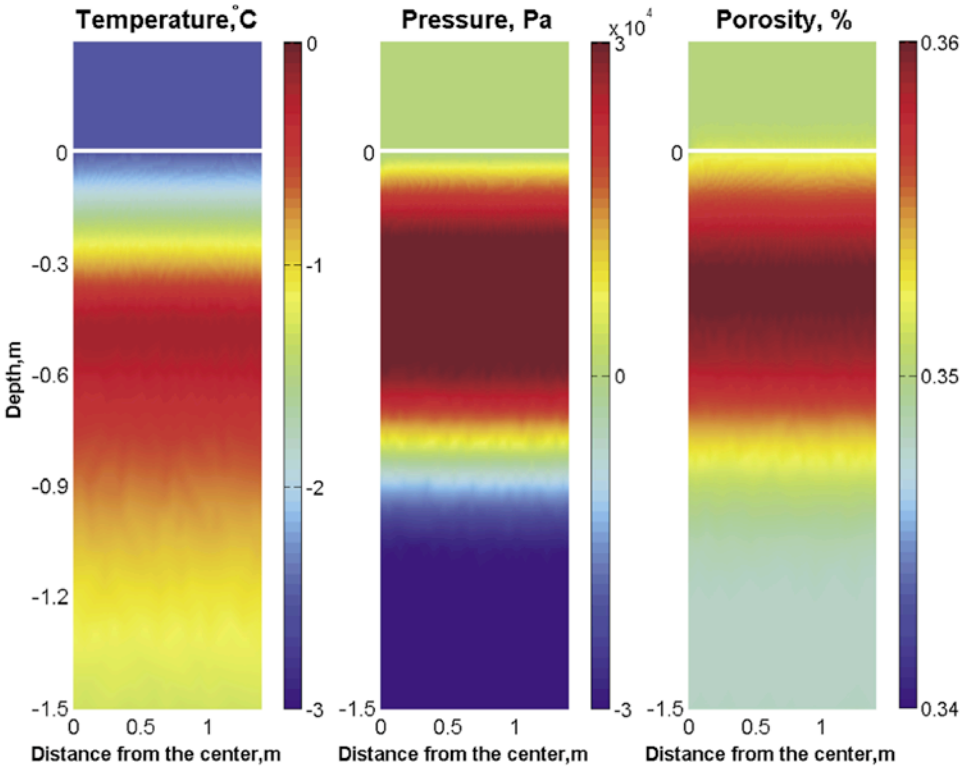

Figure 7. The temperature, pressure and soil porosity fields at the 15th day after freezing begins for the hydrologically closed system. Volumetric water expansion during freezing creates a build up of pressure in the thawed region.

in consequent ground heaving. The opposite is also true. During thawing, ice melts and consequently "some volume is being removed" from the soil, and hence the pressure decreases. Recall that for hydrologically closed systems, the mass of water in the nonsorted circle is conserved by modeling $\boldsymbol{\nu} \cdot \theta_w(\boldsymbol{v} - \boldsymbol{v}_w) = 0$ on the external boundary AB. Hence, the maximum frost heave is equal to the total volume of the "injected" material which is the difference between the final ice volume and the initial liquid-water volume. Since during freezing water expands by $\gamma = 1 - \bar{\rho}_i/\bar{\rho}_w$, or 9%, it is possible to verify whether the model conserves the total water mass. We check that the maximum frost heave is equal to γV_0, where V_0 is the volume of liquid water that became frozen at the end of simulation. To verify the model quantitatively, we consider the following four cases. In these case studies, we investigate how various soil properties affect redistribution of water resulting in the differential frost heave. Note that in all cases, the initial and boundary conditions ($T^{circle}_{surface} = T^{intercircle}_{surface}$, and $\boldsymbol{\nu} \cdot \theta_w(\boldsymbol{v} - \boldsymbol{v}_w) = 0$ on AB) are the same, but soil properties in regions 1, 2 and 3 can be different.

[31] Case 1: Homogeneous soil. We model one-dimensional freezing of a homogeneous soil which was initially thawed up to D = 0.5 meters depth. In this case, the thermal conductivities of frozen and thawed soil is 1.1 and 1.55, respectively; the hydraulic conductivity k_0 for thawed soil is 10^{-8}, the coefficient α determining the hydraulic conductivity for partially frozen soil is 5, Young's modulus is $E = 2{\cdot}10^6$ and the parameter a determining the unfrozen water content is 10^{-4}. Note that existence of the unfrozen water content leads to nonzero water flux $\mathcal{F}$, which was forcefully set to zero in the numerical program. From the physical point of view, this setting of parameters means that unfrozen water can exist in the soil pores, but the water migration is only due to nonzero gradient in the pressure p. Note that as soon as temperature becomes lower than the freezing point, ice appears, the volume occupied by water enlarges, and hence the pressure increases and exerts force onto the soil skeleton. Figure 7 shows a snap shot of temperature, pressure and soil porosity at the 15th day after the beginning of freezing. The middle plot of this Figure shows a region between 0.05 and 0.5 meters with the positive pressure increase. Note that in the region below 0.5 meters, the temperature increases, and as a result soil partially thaws, causing the decrease in the volume occupied by water, and consequently appearance of the region with negative pressure. The right plot in Figure 7 shows the snap shot of soil porosity, which depicts an increase in the initial porosity of 0.35 in the region where water freezes and a corresponding decrease where ice melts.

[32] Since the system is hydraulically closed, the maximum frost heave is equal to

$$n_0\left(1 - \frac{\bar{\rho}_i}{\bar{\rho}_w}\right)D, \tag{23}$$

where n_0 is the soil porosity at the beginning of computations. The maximum frost heave is shown in

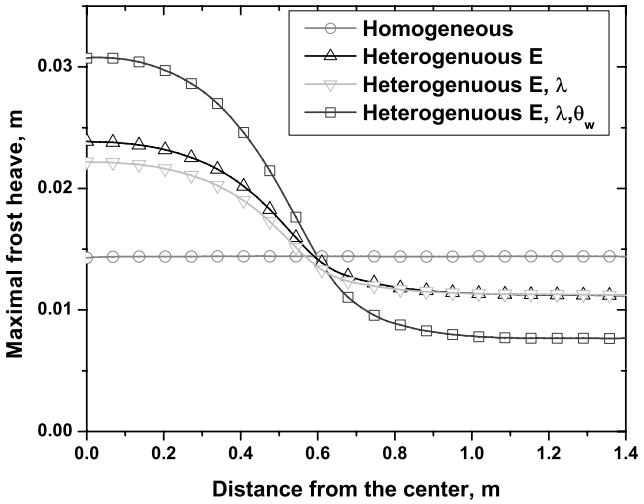

Figure 8. The maximum frost heave for different combination of rheological, thermal and hydraulic soil properties.

Figure 8, left plot. For the homogeneous soil, the frost heave is uniform and is approximately equal to $1.44 \cdot 10^{-2}$ meters, whereas the frost heave predicted by (23) is $0.55 \cdot 0.35 \cdot 0.09 \approx 1.73 \cdot 10^{-2}$ meters. Note that in derivation of the estimate (23) it was assumed that all liquid water become ice in frozen ground. Hence, the difference between the predicted and simulated frost heave is due to the presence of unfrozen liquid water in frozen soil, and is partially due to numerical errors.

[33] Case 2: Heterogeneous rheological properties. We model soil that has lenticular structure in regions 1 and 2; the value of Young's modulus E in domain *3* is larger that in domains 1 and 2, i.e. in the region 3, $E = 2 \cdot 10^7$. Different values of the Young's modulus cause water to flow from more stiff material in region 3 towards the less stiff one in the center. Note that the average value of the frost heave in this case is $1.49 \cdot 10^{-2}$ meters which is approximately the same value as for the homogeneous case, see Figure 8.

[34] Case 3: Heterogeneous rheological and thermal properties. We modify the second case by decreasing the thermal conductivity for the organic layer, regions 2, to 1.1. Distinct values of the thermal conductivity do not produce the differential frost heave with respect to the previous run. The average value of the frost heave is approximately $1.44 \cdot 10^{-2}$ meters, which is in agreement with predictions calculated by (23).

[35] Case 4: Heterogeneous rheological, thermal and hydraulic properties. We further modified the third case. We decrease the parameter a to 10^{-5} in region 2, to simulate the realistic dependence of the unfrozen water content on temperature of the organic layer. This case shows that the differential frost heave is more pronounced than in all previous runs, and there is more significant redistribution of water during freezing. The redistribution of water is related to the dependence of the hydraulic conductivity on the unfrozen water content. In the mineral soil (regions 1 and 3), the unfrozen water content is parameterized by $a = 10^{-4}$, whereas in the organic soil layer $a = 10^{-5}$. Considering that $\alpha = 5$ in (1), we have that for temperature -2 °C the hydraulic conductivity in the intercircle is more than 100 times less than in the circle. Therefore, during freezing, the migration of water through the organic layer is less than through the mineral soil, and the excessive pressure increases in the region below the organic layer forces water into the circle. This produces larger values of differential frost heave. Nevertheless, the average value of the frost heave for the entire domain is still only $1.49 \cdot 10^{-2}$ meters in this simulation.

[36] Note that on average the maximum frost heave for the entire nonsorted circle during all four simulations is the same ($\pm 0.1 \cdot 10^{-2}$ meters), and the computed differential heave is due to water redistribution only. We emphasize that the difference in Young's modulus and unfrozen water content in the circle and intercircle produce the computed differential frost heave. However, its average value is usually less than observed in the field. This is due to two factors: in these simulations, the external boundary was assumed to be water impermeable; migration caused by cryogenic suction of liquid water to the freezing front was absent in the model so far.

7. Hydraulically Open and Closed System

[37] In nature, we observe that the maximum frost heave is larger at sites where near-surface ground water is abundant [*Walker et al.*, 2004]. To explain this phenomena, we show that liquid-water migration towards the partially frozen region as well as the unlimited water supply are both essential to simulate the observed frost heave. In total, we model four different cases associated with one of the following combinations of the boundary conditions ($P = 0$, or $\boldsymbol{\nu} \cdot \theta_w(\boldsymbol{v} - \boldsymbol{v}_w) = 0$) on the external boundary and the cryogenic suction ($\mathcal{F} \neq 0$, or $\mathcal{F} = 0$). Recall that the pressure boundary condition $P = 0$ on the external boundary models flow of water in and out of the nonsorted circle, and hence the system is called hydrologically open. The condition $P = 0$ is approximated by setting $p = 0$ despite of possible artificial deformation of soil near AB that is far from the circle. Similarly, the boundary condition $\boldsymbol{\nu} \cdot \theta_w(\boldsymbol{v} - \boldsymbol{v}_w) = 0$ defines the hydrologically closed system and is imposed by setting simultaneously $\boldsymbol{\nu} \cdot \nabla p = 0$ and $\boldsymbol{\nu} \cdot \nabla T = 0$.

[38] We recall the last case in the previous section, i.e., Closed system with no suction, and the heterogeneous rheological, thermal and hydrological soil properties. In this case, the computed differential frost heave is 0.03 meters at the center of the circle and less than 0.01 meters in the intercircle, see left plot in Figure 8. However, if the boundary condition with respect to pressure on the external boundary is changed to model water flow through the boundary, or $p = 0$, we model the hydraulically open system with no suction.

[39] Case 1: Open system with no suction. Figure 9, left plot, shows the computed maximum frost heave in this case. Note that the maximum frost heave of the hydraulically open system is smaller than the one of the closed system, since positive pressure in Ω_t pushes water outside through $\partial\Omega_t$ on which $p = 0$ is modeled. These numerical experiments show that presence of a water supply at the boundary of nonsorted circle cannot alone explain the observed values of frost heave (see Figure 2).

[40] Case 2: Closed system with suction. Due to presence of the cryogenic suction $\mathcal{F} \neq 0$, there is an induced flow of

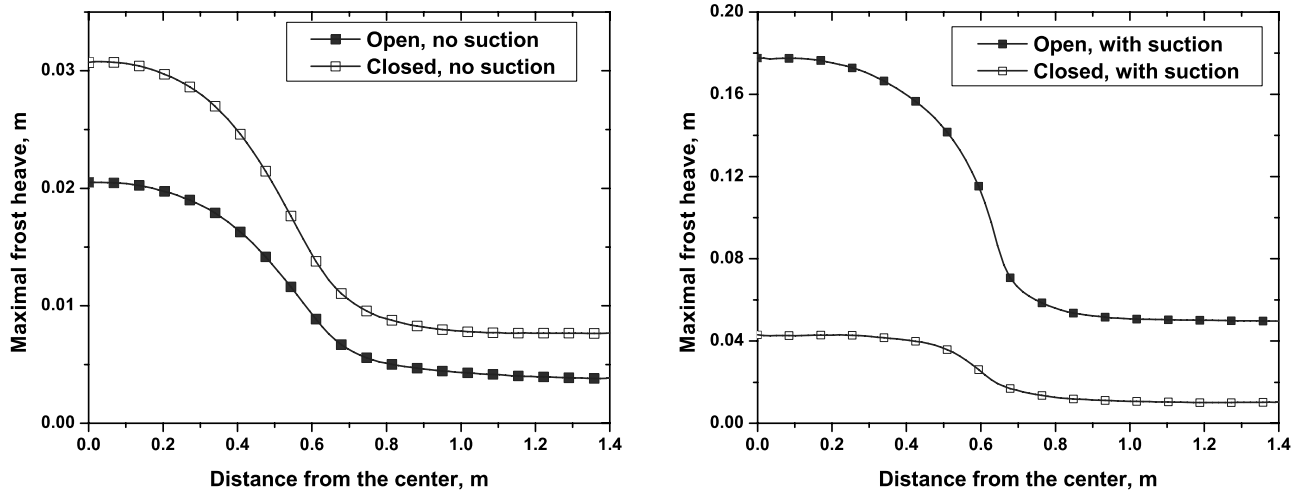

Figure 9. Maximum frost heave for hydrologically closed (left) and open (right) systems.

liquid water from the thawed region to the partially frozen zone. This causes water to move from the thawed region into the partially frozen one. As a result, the pressure p in the thawed region decreases, see Figure 10. In the hydraulically closed system without internal sources of water, the boundaries are not water permeable, and hence no additional water can appear in the nonsorted circle. Consequently, the pressure can decrease indefinitely (see Figure 10, the left plot).

[41] Case 3: Open system with suction. In the hydraulically open systems with suction, the cryogenic suction creates similar effects as in the closed systems. Namely, it forces the flow of water and creates a low pressure zone in the thawed region. However, unlike the closed systems, the pressure on the external boundary is fixed $p = 0$ and water can flow through the boundary and supply cryogenic suction forces with water in order to compensate deficiency in water volume and associated with it negative pressure. Therefore, in the hydraulically open systems, the pressure in the thawed region is slightly negative compared to the closed systems, see Figure 10, right plot. From the right plot in Figure 11, we observe that the positive pressure increase exists in the partially frozen region and it creates the uplifting forces which produce the frost heave.

[42] In this section, we have analyzed the model ((15)–(18)) and conclude that the cryogenic suction forces create water flow and also produces low pressure zones in thawed soil. However, the pressure dynamics and hence the uplifting forces strongly depend on the pressure boundary condition. The model shows that it qualitatively captures and predicts commonly occurring physical behavior of both hydraulically closed and open systems. In the next section, we analyze the model quantitatively, using some observa-

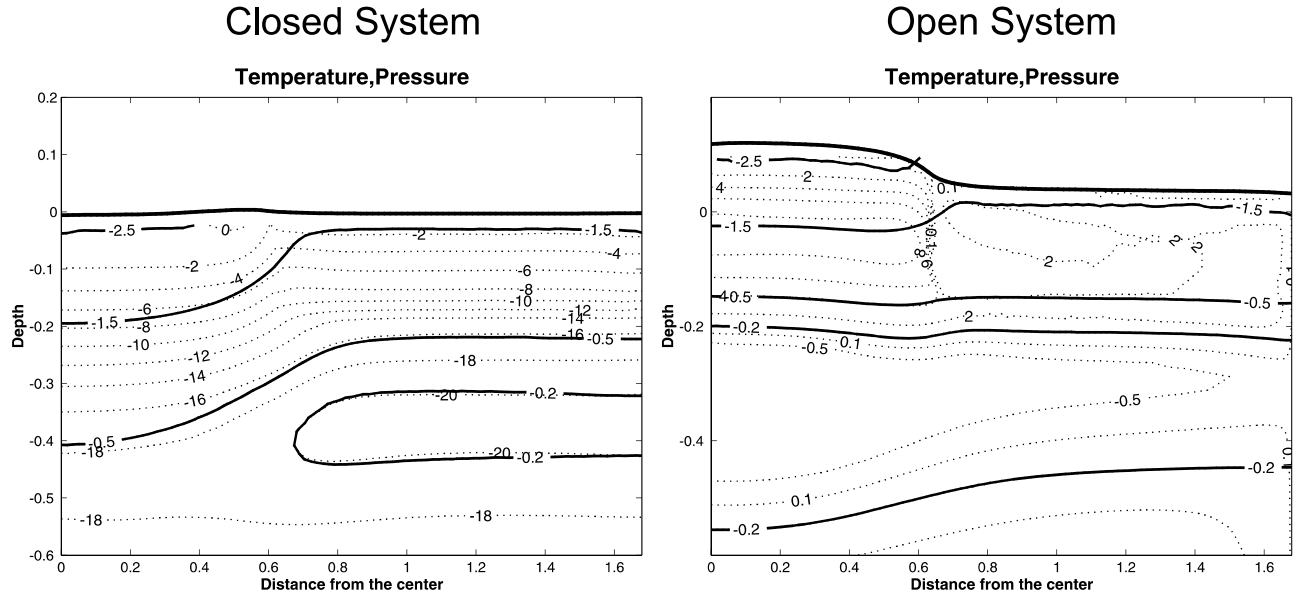

Figure 10. Contours of the temperature in °C (solid lines) and pressure in 10^5 Pa (dotted lines) at the 30th days after freezing, for hydraulically closed (left) and open (right) systems.

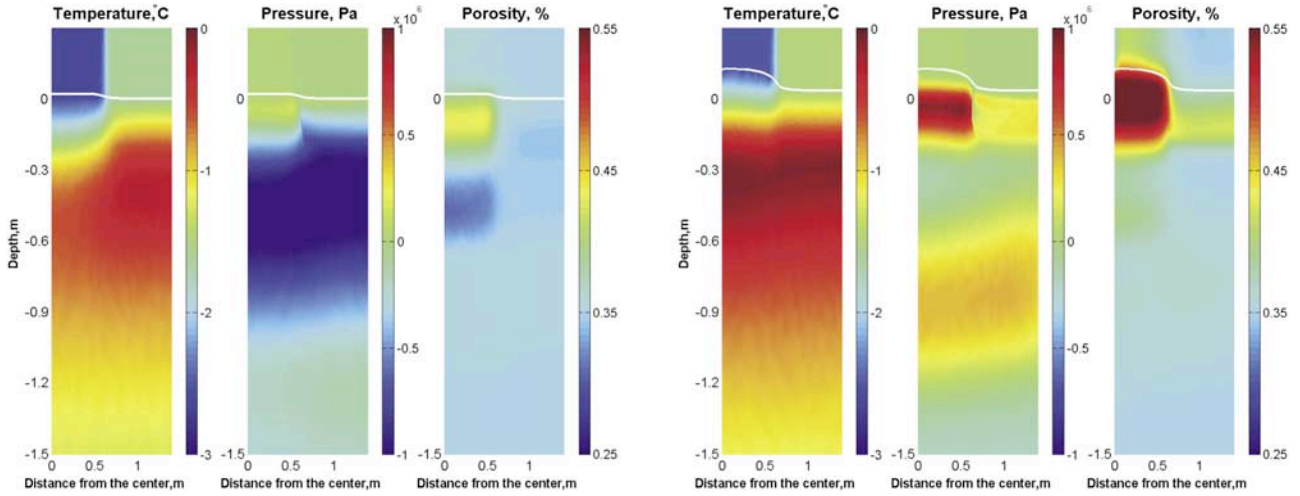

Figure 11. The temperature, pressure and soil porosity fields at the 15th day after freezing begins for the hydrologically closed (left) and open (right) system. Since the water migration through the external boundary is not permitted for closed system, the pressure decreases and becomes extremely low, whereas for open systems the migration of water compensates it and hence the uplift is created.

tions and measurements from a study site at the Franklin Bluffs, Alaska.

8. Modeling Frost Heave of a Nonsorted Circle at the Franklin Bluffs Site

[43] In this section we apply the general model given by ((15)–(18)) to a nonsorted circle located at the Franklin Bluff site on the Dalton Highway in Alaska. The nonsorted circle is approximately 0.6 meter in radius and is developed in water logged nonacidic tundra. In the intercircle, the organic layer is 0.2 meter in depth [*Walker et al.*, 2004] (G. Michaelson et al., Soil properties and patterned ground across the North American Arctic Transect: Trends in physiochemical properties, submitted to *Journal of Geophysical Research,* 2007). An array of sensors measuring temperature and moisture dynamics in time are installed at several depths and at several locations across it. However, since the measured surface temperature rapidly fluctuates, we compute its 5-day running average shown in the right plot in Figure 6 and use it as the upper boundary condition for temperature.

[44] Values of the parameter a that determines the unfrozen liquid-water content for mineral and organically enriched soil are found by fitting θ_w expressed from (11) to the measured liquid-water content at 0.35 meter depth in the circle and 0.15 meter depth in the intercircle, respectively. Thermal conductivities for the frozen mineral and organically enriched soil are set to be 1.9 and 0.9, respectively. The Young's modulus E for the mineral soil inside and outside the circle is $2{\cdot}10^6$ and $20{\cdot}10^6$, respectively, which are typical values for weakly consolidated and consolidated silt-clay mixture. Since the nonsorted circle is located in water logged area we model it as a hydraulically open system. Initial soil temperature distribution with depth was approximated by measured temperature on 09/12/2002, and the soil porosity was set to be 0.35. On this day the active-layer depths in the center of the nonsorted circle and in the surrounding tundra were 0.8 and 0.6 meter, respectively.

[45] We simulated the soil freezing from 09/12/2002 through 12/18/2002, when the temperature in the nonsorted circle became less than −5°C. The calculated liquid-water content at 0.35 meter depth in the circle and 0.15 meter depth in the intercircle are compared to the measured data (see Figure 12). The difference in timing of the modeled and observed freeze-up at each shown depth is less than 3 days. We also compare the calculated temperature dynamics to the measured one (see Figure 13). In general, the discrepancy between the measured and computed temperature at the depth of 0.35 meters in the circle is less than 1°C. However, since we utilized the smoothed surface temperature (see the

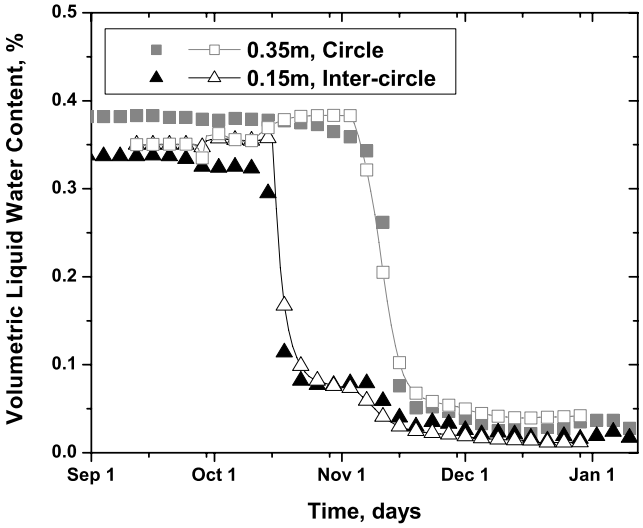

Figure 12. The dynamics of the measured (filled symbols) and computed (hollow symbols) liquid-water content θ_w at the Franklin Bluffs site at some depths in the center of the circle and in the intercircle.

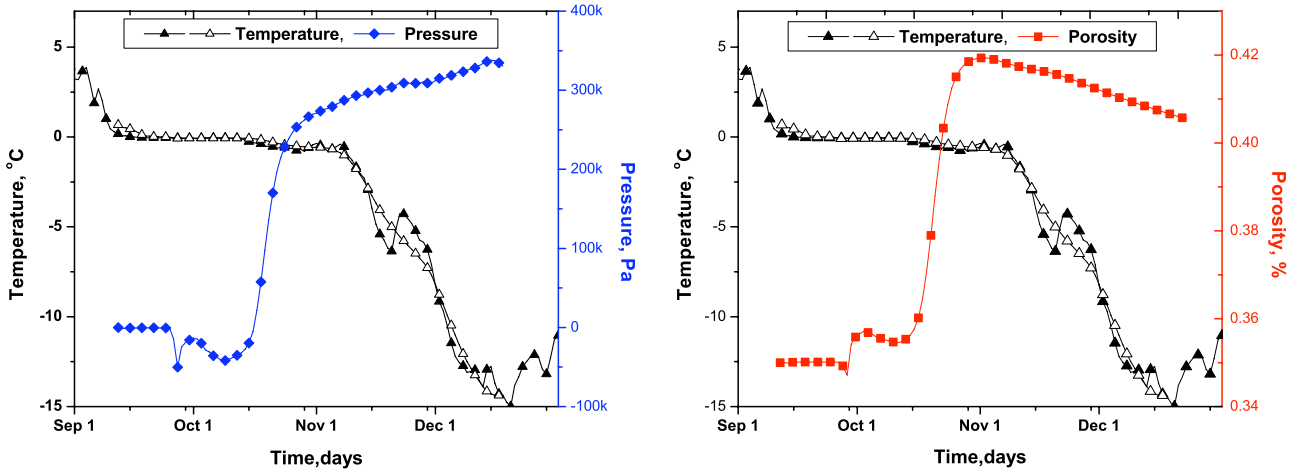

Figure 13. The dynamics of the measured (filled symbols) and calculated (hollow symbols) temperature at 0.35 meter depth in circle, respectively.

right plot in Figure 6) to force the model, we cannot resolve some details in the measured soil temperature dynamics as for example around 11/20/2002.

[46] In addition to comparing the measured and computed soil temperatures, we show the calculated pressure p dynamics at the same point, i.e. at the depth of 0.35 meters. Note that initially when the ground surface temperature was above 0°C, the pressure p was zero (we assume there is no gravity and the pressure on the lateral boundary is zero). However, as soon as ground freezing begins, the cryogenic suction starts to force water migration from a still unfrozen part of the active layer to the partially frozen one. Therefore, the pressure lowers in the entire thawed part of the active layer; the pressure dynamics has slightly negative values of p at this time which can be observed in the left plot in Figure 13. When the freezing front reaches the depth/region at which the pressure and temperature dynamics are shown (0.35 meters), the cryogenic suction starts to force water migration into this still partially frozen region. Soil porosity consecutively increases, see the right plot in Figure 13. Due to increase of the water mass, and due to its expansion while freezing the pressure p continues to increase, see the left plot in Figure 13. Note that the increased porosity is associated with formation of ice lenses and development of the frost heave (the small decrease in soil porosity is due to numerical regularization of the soil mass conservation principle). Value of the computed frost heave in the center of the nonsorted circle is approximately 0.18 meters whereas in the intercircle it is 0.045 meters. These computed values are in a good agreement with field observations, see Figure 2.

[47] In this section, we demonstrated that it is possible to simulate frost-heave dynamics of a single nonsorted circle and obtain results which are in agreement with observations. In the next section, we analyze sensitivity of the model with respect to parametrization of soil properties.

9. Sensitivity Analysis

[48] From numerical experiments, we note that the frost-heave dynamics primarily depends on several soil properties listed in Table 3. In this section, we present the results obtained from sensitivity study of the frost heave with respect to values of parameters specifying soil properties. We define the calculated frost heave at the Franklin Bluffs site as a reference point against which we compare a series of numerical experiments. In these experiments we modify thermal and hydraulic properties, and also dimensions of the nonsorted circle. In all plots the frost heave associated with the reference case, i.e. the Franklin Bluffs site, is marked by black line with circle symbols.

[49] In the first series of experiments, we analyze dependence of the frost heave on parametrization of the unfrozen water content on temperature for the mineral soil. We consider several values of the coefficient a associated with high, medium and low unfrozen water content in the soil. Note that parametrization of unfrozen water content depends on soil texture, mineralogy, solute concentration and other factors. For example, the high unfrozen water content is associated with fine-grained ground material and is modeled by large values of a, see the right plot in Figure 14. For coarse-grained materials, such as sand, the unfrozen water content sharply depends on temperature near 0°C, see plots associated with small values of a. For each shown parametrization, we simulate freezing of the nonsorted circle and compute the maximum frost heave (see the left plot in Figure 14). In these numerical experiments all model parameters except for the parametrization of the unfrozen water content were fixed and equal to the values related to the Franklin Bluffs site.

[50] From the computed results we observe that the largest frost heave occurs when soil has high unfrozen water content. This effect has the following explanation. Hydraulic conductivity k_h of the partially frozen soil increases, if the unfrozen water content θ_w becomes higher,

Table 3. Key Parameters in the Model on Which the Frost Heave Depends

Type	Parameters	Description
Hydrological	a	Parametrization of the unfrozen water content
	k_0, α	Parametrization of the hydraulic conductivity
Thermal	λ_s, C_s	Thermal conductivity and heat capacity
Rheological	E	Young's modulus

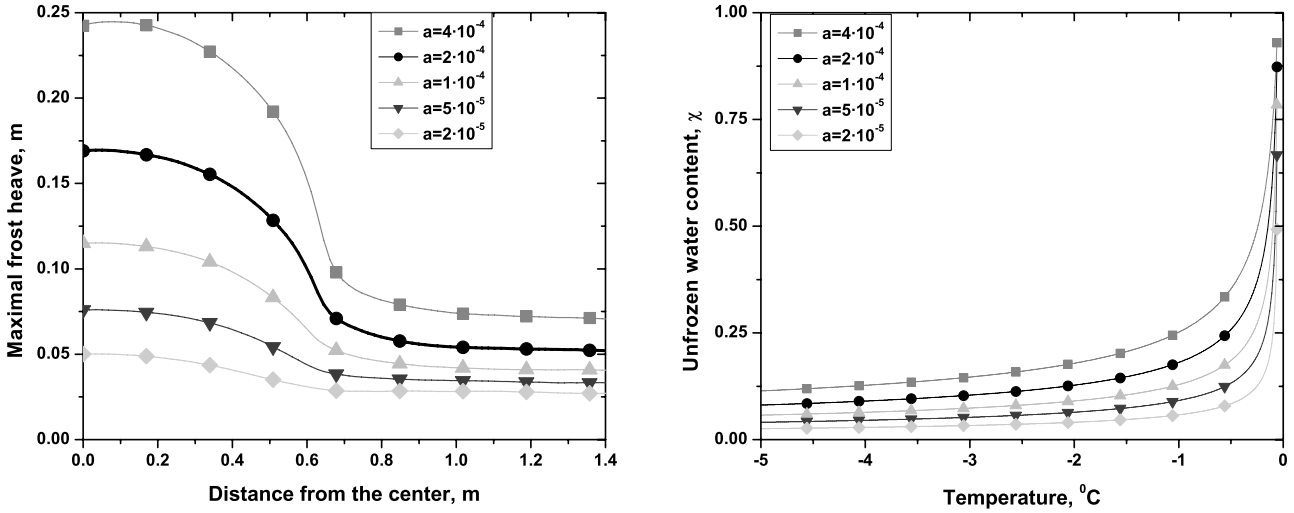

Figure 14. Sensitivity of the frost heave on parametrization of the unfrozen water content.

and hence more water migrates through the partially frozen region due to cryogenic suction flow $\mathcal{F}$ (nonlinearly dependent on θ_w and forms ice lenses. The above-mentioned dependence of the frost heave on unfrozen water content is commonly observed in nature, i.e. the sand and gravel are not frost-heave susceptible soils, whereas silt is. Note that clays, which have even higher unfrozen water content but have small hydraulic conductivity, typically are not capable developing significant frost heave.

[51] In the second series of experiments, we investigate dependence of the maximum frost heave on parametrization of hydraulic conductivity k_h for the partially frozen ground. One of the typically unknown parameters is the quantity α that determines dependence of k_h on the unfrozen liquid water content in (1). Large values of α correspond to small values of k_h, and otherwise. Figure 15 shows the computed maximum frost heave for several values of α. As in the previous experiment, we observe that the frost heave is higher when the value of k_h is larger which corresponds to smaller values of α. As in the first series of experiments, we observed that the frost heave sharply depends on the soil hydraulic properties. We note that the frost heave does not significantly depend on values of the thermal conductivity of mineral soil, as it was shown in section 6 in the third case.

[52] In our field experiments, we observe that at several sites circles have a thin horizon of the organic soil. From the physical point of view, this layer represents an additional thermal resistance and changes soil temperature regime. Therefore, in the third series of experiment, we analyze dependence of the maximum frost heave on presence of organically enriched soil in the nonsorted circles. We consider several configurations of organic layers varying in their thicknesses. We additionally place on top of the nonsorted circle an organic layer which uniformly covers the circle and intercircle. The soil thermal, hydraulic and rheological properties of this additional layer are identical to the properties of the original organically enriched soil in the intercircle for the Franklin Bluffs site. Note that increase in insulation layer causes decrease in the active-layer thickness. From our field studies, we observed that each additional 0.02–0.03 meters of the organic material results in 0.04–0.05 meter decrease of the active layer. In the left plot in Figure 16, we show the maximum frost heave developed for various thicknesses of the additional organic layer. We emphasize that observed results are in agreement with observations at nonsorted circles along the Dalton highway in Alaska. For example, the scarcely vegetated circles at the Franklin Bluff area heave by 0.15–0.20 meters, whereas moderately vegetated circles at the Happy Valley site develop only 0.07–0.10 meters of heave during winter. Also, field experiments [*Kade et al.*, 2005, 2006; *Kade and Walker*, 2008] at Sagwon Hills involved both the removal and addition of vegetation on nonsorted circles. The removal of vegetation at this location resulted in 1.4°C increase in mean summer soil temperature compared to control, and a 6% increase in the depth of the thaw layer, and a 26% increase in frost heave. The addition of 0.1 meter thick moss layer results in the opposite effect, a 2.8°C decrease in the mean summer soil surface temperature, a 15% reduction in the thaw layer, and a 52% decrease in heave. Despite the

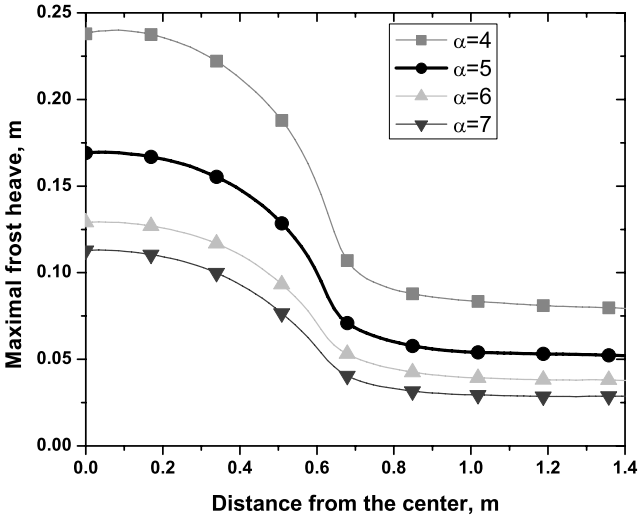

Figure 15. Sensitivity of the frost heave on parametrization of the hydraulic conductivity.

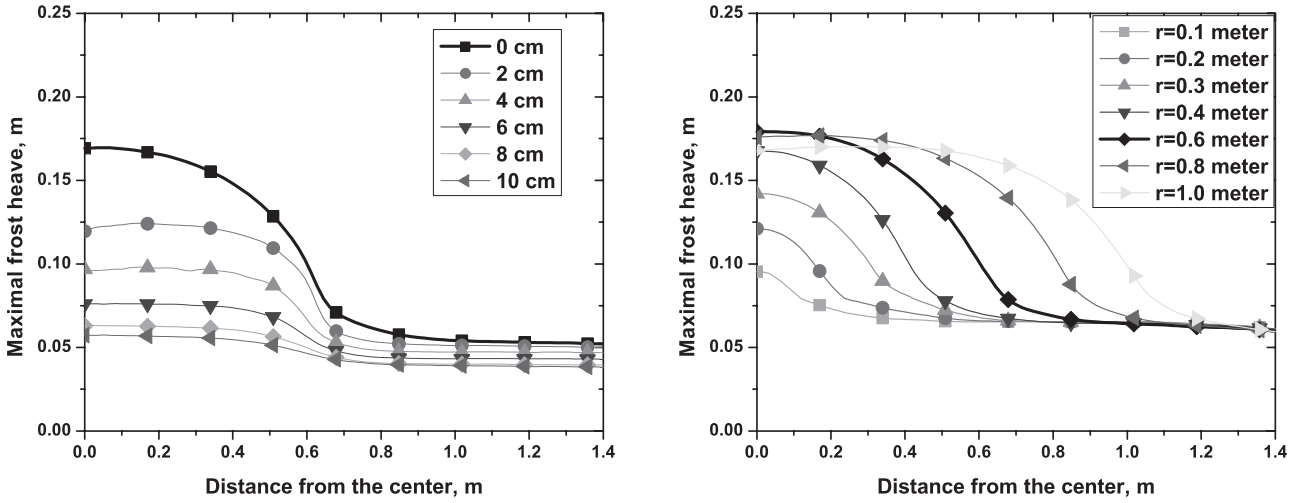

Figure 16. Sensitivity of the maximum frost heave on addition of organically enriched soil (left) and on the radius (right) of the nonsorted circle.

fact that the numerical model is focused on nonsorted circles at the Franklin Bluffs site and the field experiments were conducted at the Sagwon Hills site (these sites are only 30 kilometers apart and have similar soil and climate conditions), results from these studies show qualitative agreement, and similar quantitative behavior of frost-heave reduction.

[53] In the fourth series of experiments, we investigate sensitivity of frost heave on the radius of the nonsorted circles. We calculate the frost heave for circles which have 0.1, 0.2, 0.3, . . ., 1.0 meter radius. Our calculations support observations which reveal that small scale nonsorted circles heave less comparing to the large diameter ones. The maximum computed frost heave is for circles with the radius of 0.6 meters, see the right plot in Figure 16. For circles with the radius larger than 0.6 meters, the maximum frost heave slightly decreases since liquid water has to migrate to the center of the nonsorted circle longer from the lateral boundary where water is abundant. Smaller values of the frost heave, that is computed in the center of the nonsorted circle with a large radius, can promote development of live vegetation.

10. Conclusions

[54] We present a numerical thermo-mechanical model of differential frost heave with special emphasis on simulating biocomplexity of nonsorted circle ecosystems. Unlike other models that study 1-D ice-lens formation, we consider the 2-D effects of soil freezing. Heterogeneity in soil properties and surface conditions result in a differential frost penetration and 2-D temperature fields. Therefore, the cryogenic suction results in horizontal water redistribution between intercircle and circle areas. Despite the simplicity (no diffusion of salts, simplified rheology) the model captures and successfully simulates temperature and water dynamics in soil. Also, the model satisfactorily simulates the ground surface motion in relation to frost heave and explains the dependence of the amount of frost heave on specific environmental properties of this ecosystem.

[55] Model was tested using observational data obtained from several sites within the Permafrost/Ecological North American Arctic Transect. We obtained a good comparison between simulated and observed dynamics of physical processes in the nonsorted circle at the Franklin Bluffs. The model also qualitatively represents "nonheaving" nonsorted circles at the Howe Island site.

[56] The simulated frost heave is sensitive to hydrological soil properties, and to change in the vegetative insulation layer within the circle and intercircle areas. The results of our sensitivity analysis with respect to addition/removal of vegetation layer to/from the surface of a circle are well correlated with field observations, where a layer of organic material was added to the nonsorted circle, or removed. The performed sensitivity analysis provides deeper understanding of functioning of the nonsorted circle as an ecosystem.

[57] Based on results from the sensitivity analysis, we conclude that the most active development of differential frost heave takes place for nonsorted circles within waterlogged area with strong upper-soil-layer heterogeneity caused by living vegetation. The most important driver of the nonsorted circle ecosystem is the presence of vegetation that, over a significant time, changes the soil mineralogy and thermal and hydrological soil properties, thus changing the amount of differential frost heave and reducing or enhancing all biogeophysical processes responsible for the formation and evolution of the nonsorted circles.

[58] Testing of our numerical model provides an assurance that this model can be used to study the impact of changes in major natural geophysical and biological drivers on specific properties and dynamics of the nonsorted circles in different ecological systems. The presented model provides a very powerful tool to investigate possible future changes in this ecosystem in relation to observed and projected climatic and biological changes in the Arctic.

[59] **Acknowledgments.** We would like to thank Jacob Stroh, Michael Ladouceur, Juha Hartikainen, and Lynn Bennethum for their advice, critique and reassurances along the way. We are thankful to reviewers who helped to clarify certain parts of this manuscript. This research was funded by ARCSS Program and by the Polar Earth Science Program, Office of Polar Programs, National Science Foundation (OPP-

0120736, ARC-0632400, ARC-0520578, ARC-0612533, IARC-NSF CA: Project 3.1 Permafrost Research), by NASA Water and Energy Cycle grant, and by the State of Alaska.

References

Astrakhantcev, G. (1978), Method of fictitious domains for a second-order-elliptic equation with natural boundary conditions, *USSR Comput. Math. Math. Phys.*, *18*, 114–121.

Bennethum, L., and T. Weinstein (2004), Three pressures in porous media, *Transp. Porous Media*, *54*(1), 1–34.

Beskow, G. (1935), *Soil Freezing and Frost Heaving With Special Application to Roads and Railroads, C, no. 375, Year Book no. 3*, Swedish Geol. Soc., Technol. Inst., Northwestern Univ., translated by J. O. Osterberg.

Blanchard, D., and M. Fremond (1982), Cryogenic suction in soils, in *Proceedings of the Third International Symposium on Ground Freezing*, vol. 1, pp. 233–238, Hanover, N. H.

Buzbee, B., F. Dorr, J. George, and G. Golub (1971), The direct solution of the discrete poisson equation on irregular regions, *SIAM J. Numer. Anal.*, *8*, 722–736.

Coussy, O. (2005), Poromechanics of freezing materials, *J. Mech. Phys. Solids*, *53*, 1689–1718.

Dash, J., H. Fu, and J. Wettlaufer (1995), The premelting of ice and its environmental consequences, *Rep. Prog. Phys.*, *58*, 115–167.

de Vries, D. (1963), Physics of the plant environment, in *Thermal Properties of Soils*, edited by W. R. van Wijk, pp. 210–235, Wiley, New York.

Everett, D. (1961), The thermodynamics of frost damage to porous solid, *Trans. Faraday Soc.*, *57*, 1541–1551.

Fowler, A. (1989), Secondary frost heave in freezing soils, *SIAMJ. Appl. Math.*, *49*, 991–1008.

Fremond, M., and M. Mikkola (1991), Thermomechanical modeling of freezing soil, in *Proceedings of the 6th International Symposium on Ground Freezing*, edited by W. C. Yu, pp. 17–24, Balkema, Rotterdam.

Glowinski, R., T.-W. Pan, and J. Periaux (1994), Fictitious domain method for dirichlet problems and applications, *Comput. Methods Appl. Mech. Eng.*, *111*, 283–303.

Graham, J., and V. Au (1985), Effects of freeze-thaw and softening on a natural clay at low stresses, *Can. Geotech. J.*, *22*(1), 69–78.

Hartikainen, J., and M. Mikkola (1997), General thermomechanical model of freezing soil with numerical applications, in *Ground Freezing*, pp. 101–105, Balkema, Rotterdam.

Hobbs, P. (1974), *Ice Physics*, Clarendon Press, Oxford.

Huyghe, J., R. V. Loon, and F. Baaijens (2004), Fluid-solid mixtures and electrochemomechanics: the simplicity of lagrangian mixture theory, *Comput. Appl. Math.*, *23*(2–3), 235–258.

Jussila, P. (2006), Thermodynamics of porous media - I: thermohydraulic model for compacted bentonite, *Transp. Porous Media*, *62*, 81–107.

Kade, A., and D. Walker (2008), Experimental alternation of vegetation on nonsorted circles: effects on cryogenic activity and implications for climate change in the Arctic, *Arct. Antarct. Alp. Res.*, in press.

Kade, A., D. Walker, and M. Raynolds (2005), Plant communities and soils incryoturbated tundra along a bioclimate gradient in the Low Arctic, Alaska, *Phytocoenologia*, *35*, 761–820.

Kade, A., V. Romanovsky, and D. Walker (2006), The n-factor of nonsorted circles along a climate gradient in arctic Alaska, *Permafrost Periglacial Processes*, *17*, 279–289.

Konrad, J., and C. Duquennoi (1993), A model for water transport and ice lensing in freezing soils, *Water Resour*, *29*(9), 3109–3124.

Konrad, J., and N. Morgenstern (1981), The segregation potential of a frozen soil, *Can. Geotech. J.*, *18*, 482–491.

Kuznetsov, Y. (2000), The fictitious domain method, in *Proceedings of the Annual International Meeting on Domain Decomposition Methods*, edited by M. Garbey, Lyon.

Landau, L., and E. Lifshitz (1969), *Statistical Physics*, Addison-Wesley, Boston, Mass.

Li, N., F. Chen, B. Su, and G. Cheng (2002), Theoretical frame of the saturated freezing soil, *Cold Reg. Sci. Technol.*, *35*, 73–80.

Litvan, G. (1972), Phase transitions of absorbates iv. mechanism of frost hardened cement paste, *J. Am. Ceram. Soc.*, *55*(1), 38–42.

Marchuk, G., Y. Kuznetsov, and A. Matsokin (1986), Fictitious domain and domain decomposition methods, *Sov. J. Numer. Anal. Math. Model.*, *1*, 1–82.

Michalowskin, R., and M. Zhu (2006), Frost heave modeling using porosity rate function, *Int. J. Numer. Anal. Methods Geomech.*, *30*, 703–722.

Mikkola, M., and J. Hartikainen (2001), Mathematical model of soil freezing and its numerical application, *Int. J. Numer. Methods Eng.*, *52*, 543–557.

O'Neill, K., and R. Miller (1985), Exploration of a rigid ice model of frost heave, *Water Resour. Res.*, *21*, 281–296.

Penner, E. (1959), The mechanism of frost heave in soils, *Highway Res. Board Bull.*, *225*, 1–22.

Peterson, R., and W. Krantz (2003), A mechanism for differential frost heave and its implications for patterned ground formation, *J. Glaciol.*, *49*(164), 69–80.

Powers, T., and R. Helmuth (1953), Theory of volume changes in hardened portland cement paste during freezing, in *Proceedings of the Highway Research Board*, vol. 32, pp. 285–297, Washington, D. C.

Qi, J., P. Vermeer, and G. Cheng (2006), A review of the influence of freeze-thaw cycles on soil geotechnical properties, *Permafrost Periglacial Processes*, *17*, 245–252.

Ramiere, I., P. Angot, and M. Belliard (2005), Fictitious domain methods to solve convection-diffusion problems with general boundary conditions, in *Proceedings of 17th Computational Fluid Dynamics Conference*, pp. 2005–4709, AIAA, Toronto.

Rempel, A., J. Wettlaufer, and M. Worster (2004), Premelting dynamics in a continuum model of frost heave, *J. Fluid Mech.*, *498*, 227–244.

Samarskii, A., and P. Vabishchevich (1996), *Computational Heat Transfer, Mathematical Modeling*, vol. 1, Wiley, New York.

Saulev, V. (1963), On solution of some boundary value problems on high performance computers by fictitious domain method (in Russian), *Siberian Math. J.*, *4*(4), 912–925.

Sergueev, D., G. Tipenko, V. Romanovsky, and N. Romanovsky (2003), Mountain permafrost thickness evolution under influence of long-term climate fluctuations (results of numerical simulation), in *Proceedings of the Eighth International Conference on Permafrost*, vol. 2, edited by M. Phillips, S. Springman, and L. Arenson, pp.1017–1021.

Taber, S. (1918), Ice forming in clays will lift surface weights, *Eng. News Record*, *80*(6), 262–263.

Taber, S. (1929), Frost heaving, *J. Geol.*, *37*, 428–461.

Taber, S. (1930), The mechanics of frost heaving, *J. Geol.*, *38*(4), 303–317.

Tsytovich, N. (1975), *Mechanics of Frozen Ground*, Scripta.

van Everdingen, R. (2002), *Multi-Language Glossary of Permafrost and Related Ground-Ice Terms*, Natl. Snow and Ice Data Cent./World Data Cent. for Glaciol., Boulder, Colo.

Viklander, P., and D. Eigenbrod (2000), Stone movements and permeability changes in till caused by freezing and thawing, *Cold Reg. Sci. Technol.*, *31*(2), 151–162.

Walker, D., et al. (2004), Frost-boil ecosystems: Complex interactions between landforms, soils, vegetation and climate, *Permafrost Periglacial Processes*, *15*, 171–188.

Walker, D., et al. (2008), Arctic patterned-ground ecosystems: A synthesis of studies along a North American Arctic Transect, *J. Geophys. Res.*, doi:10.1029/2007JG000504, in press.

Watanabe, K., and M. Mizoguchi (2000), Ice configuration near a growing ice lens in a freezing porous medium consisting of micro glass particles, *Crystal Growth, J.*, *213*, 135–140.

Wettlaufer, J., and M. Worster (1995), Dynamics of premelted films: Frost heave in a capillary, *Phys. Rev. E*, *51*, 4679–4689.

Williams, P. (1982), *The Surface of the Earth: An Introduction to Geotechnical Science*, Longman, London.

Williams, P., and M. Smith (1989), *The Frozen Earth*, Cambridge Univ. Press, Cambridge.

Zienkiewicz, O., and R. Taylor (1991), *The Finite Element Method*, vol. 1, McGraw-Hill, London.

D. J. Nicolsky and V. E. Romanovsky, Geophysical Institute, University of Alaska Fairbanks, P.O. Box 757320, Fairbanks, AK 99775, USA. (ftdjn@uaf.edu)

G. S. Tipenko, Institute of Environmental Geoscience, Russian Academy of Science, 13-2 Ulansky pereulok, P.O. Box 145, 101000 Moscow, Russia.

D. A. Walker, Institute of Arctic Biology, University of Alaska Fairbanks, P.O. Box 757000, Fairbanks, AK 99775, USA.